Published in final edited form as:
J Immunol. 2010 November 1; 185(9): 5607–5618. doi:10.4049/jimmunol.1001984.

Enhanced Antiviral T Cell Function in the Absence of B7-H1 is Insufficient to Prevent Persistence but Exacerbates Axonal Bystander Damage during Viral Encephalomyelitis[1]

Timothy W. Phares[*], **Stephen A. Stohlman**[*], **David R. Hinton**[†], **Roscoe Atkinson**[†], and **Cornelia C. Bergmann**[2,*]

[*]Department of Neurosciences, Lerner Research Institute, The Cleveland Clinic, Cleveland, OH 44195, USA

[†]Department of Pathology, Keck School of Medicine, University of Southern California, Los Angeles, CA 90033, USA

Abstract

The T cell inhibitory ligand B7-H1 hinders T cell-mediated virus control, but also ameliorates clinical disease during autoimmune and virus induced CNS disease. In mice infected with glia-tropic demyelinating coronavirus, B7-H1 expression on oligodendroglia delays virus control, but also dampens clinical disease. To define the mechanisms by which B7-H1 alters pathogenic outcome, virus infected B7-H1 deficient (B7-H1$^{-/-}$) mice were analyzed for altered peripheral and CNS immune responses. B7-H1 deficiency did not affect peripheral T or B cell activation, nor alter the magnitude or composition of CNS infiltrating cells. However, higher levels of IFN-γ mRNA in CNS infiltrating virus-specific CD8 T cells as well as CD4 T cells contributed to elevated IFN-γ protein in the B7-H1$^{-/-}$ CNS. Increased effector function at the single cell level was also evident by elevated granzyme B expression specifically in virus-specific CNS CD8 T cells. Although enhanced T cell activity accelerated virus control, 50% of mice succumbed to infection. Despite enhanced clinical recovery, surviving B7-H1$^{-/-}$ mice still harbored persisting viral mRNA, albeit at reduced levels compared to wild-type mice. B7-H1$^{-/-}$mice exhibited extensive loss of axonal integrity although demyelination, a hallmark of virus induced tissue damage, was not increased. The results suggest that B7-H1 hinders viral control in B7-H1 expressing glia cells, but does not mediate resistance to CD8 T cell-mediated cytolysis. These data are the first to demonstrate that B7-H1-mediated protection from viral induced immune pathology associated with encephalomyelitis resides in limiting T cell-mediated axonal bystander damage, rather than direct elimination of infected myelinating cells.

Keywords

neuroimmunology; viral; rodent; inflammation; T cells

[1]This work was supported by National Institutes of health grants NS 18146, NS064932 and AI 47249.

[2]Address correspondence and reprint request to: Dr. Cornelia C. Bergmann, Department of Neuroscience, Lerner Research Institute, The Cleveland Clinic, 9500 Euclid Avenue, NC30, Cleveland, OH 44195, Phone: 216-444-5922, Fax: 216-444-7927, bergmac@ccf.org.

Disclosures The authors have no financial conflict of interest.

Introduction

Effector T cells are regulated by a number of soluble as well as contact dependent mechanisms that limit excessive activation and overt immune-mediated damage. Programmed death-1 (PD-1) receptor and its ligand B7-H1, also known as PD-L1, are among the negative regulators that can deliver inhibitory signals to both CD4 and CD8 lymphocytes in a target dependent manner (1). PD-1 is up-regulated on T cells, B cells (2), NK cells (3) and monocytes/macrophages (4, 5) upon activation. B7-H1 is expressed on lymphocytes, macrophages, dendritic cells and a variety of non-hematopoietic cell types (6-14). While B7-H1 expression is constitutive in some cell types, it is inducible on most non-hematopoietic cells by type I and II IFN (6, 9-11, 13-15). PD-1:B7-H1 interactions can modulate both Th1 and Th2 responses by dampening proliferation, cytokine production and cytolytic activity (11, 13, 16-25). Blockade of PD-1:B7-H1 interactions via genetic deletion or Ab treatment results in enhanced immunopathology (12, 26-28). For example, transformation of a mild transient myocarditis into a lethal disease by B7-H1 Ab blockade demonstrates the critical role of B7-H1 expression on cardiac endothelial cells in regulating CD8 T cell-mediated heart injury (27). PD-1:B7-H1 blockade during HSV type 1 infection accelerates the development and severity of herpetic stromal keratitis, correlating with increased CD4 T cell proliferation and IFN-γ secretion (28). Furthermore, more rapid clearance of adenovirus from the liver in the absence of PD-1 is associated with increased hepatocellular injury attributed to enhanced CD4 and CD8 lymphocyte proliferation (18). These studies all confirm the PD-1:B7-H1 pathway as a key determinant in counteracting destructive T cell effector activity. On the other hand, down-regulation of virus-specific T cell responses by PD-1:B7-H1 interactions contributes to establishment and limited control of persistent virus infections (17, 19, 21, 25, 29-33).

PD-1:B7-H1 interactions have been extensively studied in peripheral antiviral immunity; however, contributions of direct target cell interactions versus bystander effects on tissue damage have not been established. Furthermore, their detrimental or protective function during neurotropic infections is poorly characterized. Resident cells of the CNS do not constitutively express B7-H1 (6-8, 10, 12). Nevertheless, B7-H1 is induced in the CNS under inflammatory conditions such as viral encephalitis (6, 10) and experimental allergic encephalomyelitis (EAE) (12). However, little is known about the regulation of B7-H1 expression in distinct CNS resident cell types and its subsequent effects on T cell function. Following peripheral rabies virus infection B7-H1 expression on neurons prevents viral control resulting in neuroinvasion, enhanced CNS viral load, and mortality (6). B7-H1 also limits the control of neurotropic coronavirus within the CNS, but, conversely, reduces morbidity (10). Infection by the nonlethal, glia-tropic mouse coronavirus hepatitis virus strain JHM (JHMV), induces an encephalomyelitis that leads to a persistent CNS infection predominantly in spinal cords with ongoing myelin loss in wild-type (wt) mice (34-37). The minimal virus replication in astrocytes and microglia is predominantly controlled by perforin-mediated CD8 T cell cytolysis, while IFN-γ controls viral replication in oligodendroglia, the major target of virus infection (38-41). Virus-specific CD8 T cells infiltrating the CNS express high levels of PD-1, while B7-H1 is prominently up-regulated on oligodendroglia, and to a lesser extent on microglia and astrocytes (10). Evasion of T cell function by B7-H1 expression on oligodendroglia is supported by accelerated reduction of viral mRNA and Ag in infected B7-H1 deficient (B7-H1$^{-/-}$) compared to wt mice (10).

To understand the mechanisms underlying the discrepancy between increased viral control yet increased morbidity during JHMV infection, this study examined the affects of B7-H1 deficiency on T cell expansion and function within the CNS. B7-H1 deficiency affected neither peripheral virus-specific T cell expansion, nor the numbers or composition of CNS infiltrating cells. However, enhanced IFN-γ production by both CD8 and CD4 T cells within

the CNS, in addition to enhanced granzyme B expression by virus-specific CD8 T cells demonstrated increased T cell effector function. Elevated and prolonged IFN-γ secretion further correlated with sustained mRNA encoding inducible nitric oxide synthase (iNOS) and TNF, as well as microglia/monocyte-derived macrophage activation and increased axonal damage. The absence of increased myelin loss suggested B7-H1 does not protect oligodendrocytes directly from immune attack, but rather dampens ongoing immune activation. The results demonstrate that modulation of T cell effector functions leads to detrimental bystander effects on non-infected cell types, despite more effective viral control. The data further question the goal of reducing viral load in the CNS using T cell based strategies prior to understanding how distinct infected cell types contribute to T cell regulation.

Materials and Methods

Mice and virus infection

Wt C57BL/6 mice were purchased from the National Cancer Institute (Frederick, MD). B7-H1$^{-/-}$and transgenic mice expressing GFP via the oligodendroglia specific proteolipid protein promoter on the C57BL/6 background were previously described (42, 43). All mice were bred under pathogen-free conditions at an accredited facility at the Cleveland Clinic Lerner Research Institute. Mice were infected at 6-7 wks of age by intracranial injection with either 250 PFU of the glia-tropic JHM variant V2.2-1 of mouse hepatitis virus (JHMV) or 500 PFU of a dual monoclonal Ab (mAb)-derived JHMV variant designated V2.2/7.2-2 (44). Animals were scored daily for clinical signs of disease with: 0, healthy; 1, ruffled fur and hunched back; 2, hind limb paralysis or inability to turn to upright position; 3, complete hind limb paralysis and wasting; 4, moribund or dead. All procedures were conducted in accordance with federal guidelines under animal protocols approved by the Institutional Animal Care and Use Committees.

Isolation of mononuclear cells

CNS-derived mononuclear cells were isolated as described previously (34). Briefly, brains (n = 3-6) were homogenized in ice-cold Tenbroeck glass grinders in Dulbecco's PBS. Homogenates were clarified by centrifugation and supernatants collected and stored at -80°C for further analysis. Cell pellets were resuspended in RPMI supplemented with 25 mM HEPES, adjusted to 30% Percoll (Pharmacia, Piscataway, NJ) and underlayed with 1ml 70% Percoll. After centrifugation at 800 × g for 30 min at 4°C, cells were recovered from the 30%-70% interface, washed once and resuspended in FACS buffer (PBS with 0.5% BSA). Cell suspensions from cervical lymph nodes (CLN) were prepared from identical animals as previously described (34). For PCR analysis of purified CD45^{lo} microglia, CNS monocyte-derived CD45^{hi}CD11b^{+} macrophages and CD45^{-}GFP^{+} oligodendroglia were isolated from infected mice following trypsin digestion as previously described (10). In brief, pooled brain or spinal cords (n = 6) were finely minced and digested with 0.25% trypsin in PBS for 30 minutes at 37°C. Trypsin activity was terminated by addition of 20% Newborn Calf Serum followed by Percoll gradient centrifugation as described above.

Flow cytometric analysis and fluorescence activated cell sorting

Cells were incubated with mouse serum and rat anti-mouse FcγIII/II mAb (2.4G2; BD Bioscience, San Diego, CA) for 20 min on ice prior to staining. Expression of cell surface markers was determined by incubation of cells with FITC-, PE-, PerCP-, or allophycocyanin-conjugated mAb specific for CD45 (30-F11), CD4 (L3T4), CD8 (53-6.7), CD11b (M1/70), CD25 (PC61), CD62L (MEL-14) (BD Bioscience, San Jose, CA) and PD-1 (RMP1-30) (eBioScience San Diego, CA) for 30 minutes on ice. Virus-specific CD8^{+} T cells were identified using D^{b}/S510 MHC class I tetramers (Beckman Coulter Inc.,

Fullerton, CA) as described previously (34). Stained cells were washed twice with FACS buffer and fixed in 2% paraformaldehyde. For intracellular detection of granzyme B and Foxp3 cells were stained for cell surface markers prior to permeabilization with either Cytofix/Cytoperm Reagent (BD PharMingen) or Fixation/Permeabilization Reagent (eBioScience) and staining with allophycocyanin-labeled anti-granzyme B (GB12, isotype-control mouse IgG1; Caltag Laboratories Burlingame, CA) or FITC-labeled anti-Foxp3 (FJK-16s; eBioScience), respectively. A minimum of 2×10^5 viable cells were stained and analyzed on a FACSCalibur flow cytometer (BD, Mountain View, CA). Data were analyzed using FlowJo software (Tree Star Inc., Ashland, OR). CNS monocyte-derived $CD45^{hi}CD11b^{+}$ macrophages, $CD45^{lo}$ microglia, $CD45^{-}GFP^{+}$ oligodendroglia, CD4 T cells as well as $tetramer^{+}$ and $tetramer^{-}$ CD8 T cells were purified from pooled brain or spinal cords (n = 6) using a BD FACSAria (BD Bioscience). A minimum of 10^5 cells were collected per pooled sample and frozen in 400μl of Trizol (Invitrogen, Carsbad, CA) at -80 °C for subsequent RNA extraction and PCR analysis as described previously (45).

Virus titers and cytokine determination

Virus titers within the CNS were determined in clarified supernatants by plaque assay using the murine DBT astrocytoma as detailed previously (44). Plaques were counted after 48 hr incubation at 37°C. Clarified supernatants were also used to measure IFN-γ and IL-10 by ELISA as previously described (10, 46). Briefly, 96 well plates were coated overnight at 4°C with 100μl of 1μg/ml of anti-IFN-γ (R4-6A2; BD Bioscience) or 3.5μg/ml anti-IL-10 (JES5-2A5, BD Bioscience). Non-specific binding was blocked with 10% FCS in PBS for 1.5 hr before the addition of IFN-γ or IL-10 recombinant cytokine standard (BD Bioscience) and samples. After a 2 hr incubation at room temperature bound IFN-γ or IL-10 was detected using biotinylated anti-IFN-γ (XMG1.2, BD Bioscience) or anti-IL-10 (JES5-I6E3, BD Bioscience) and avidin peroxidase followed by 3,3',5,5' Tetramethylbenzidine (TMB Reagent Set; BD Bioscience) 1 hr later. Optical densities were read at 450nm in a Bio-Rad Model 680 microplate reader and analyzed using Microplate Manager 5.2 software (Bio-Rad Laboratories, Hercules, CA). Titers were calculated as reciprocals of the highest dilution that exceeded three standard deviations over the mean negative control.

Histopathology

Tissues were fixed in 10% formalin and embedded in paraffin. Distribution of viral Ag was determined by immunoperoxidase staining using the anti-JHMV mAb J.3.3 as the primary Ab, horse anti-mouse as secondary Ab and 3,3′-diaminobenzidine substrate (Vectastain-ABC kit; Vector Laboratories, Burlingame, CA). For enumeration of Ag positive cells sections were digitized using the Automated Cellular Imaging System Software (Dako, Carpinteria), counted manually and reported as positive cells/mm^2. Demyelination was determined by staining with luxol fast blue (LFB) while axonal integrity was examined using anti-phosphorylated neurofilament mAb SMI-31 and anti-nonphosphorylated neurofilament mAb SMI-32 (Covance, Princeton, NJ). Percentage area of demyelination in LFB stained sections were determined as previously described (40). Oligodendrocytes were identified with anti-adenomatous polyposis coli (APC) mAb (OP80, Calbiochem). Apoptotic cells were identified with anti-activated caspase-3 Ab (Asp175; Cell Signaling, Beverly, MA). Microglia and infiltrating monocytes were identified using anti-ionized calcium-binding adapter molecule-1 Ab (Iba-1), while anti-CD3 Ab (Abcam, Cambridge, MA) detected T cells. Sections were scored in a blinded fashion and representative fields were identified based on average score of all sections in each experimental group.

Virus-specific Abs

Sera from JHMV infected mice were assessed for virus-specific Abs by ELISA as previously described (47, 48). Briefly, plates were coated with 100 μl of a serum free

supernatant derived from JMHV infected DBT cells and incubated overnight at 4°C. Plates were washed with PBS containing 0.05% Tween 20 and blocked with 10% FCS in PBS for 1 hr before adding samples. Samples were diluted 2 fold in PBS and incubated overnight at 4°C. Plates were then washed and bound Ab was detected using biotinylated goat anti-mouse IgG (Jackson ImmunoResearch Laboratories,West Grove, PA), avidin peroxidase and 3,3',5,5' Tetramethylbenzidine (BD Bioscience). Absorbance was read at 450nm in a Bio-Rad Model 680 microplate reader and analyzed using Microplate Manager 5.2 software (Bio-Rad Laboratories, Hercules, CA).

PCR

Snap frozen brains, spinal cords or livers from individual mice (n = 3-4) were placed into 1 ml Trizol (Invitrogen) and homogenized in Tenbroeck glass grinders. RNA was isolated as previously described (49). DNA contamination was removed by treatment with DNase I for 30 min at 37°C (DNA-free kit, Ambion, Austin, TX) and cDNA was synthesized from RNA using M-MLV Reverse Transcriptase (Invitrogen) and oligo-dT primers (Promega Madison, WI). Quantitative real-time PCR was performed using 4 μl of cDNA and SYBR Green Master Mix (Applied Biosystems, Foster City, CA) in duplicate on a 7500 Fast Real-Time PCR System (Applied Biosystems). PCR conditions were 10 min at 95°C followed by 40 cycles at 95°C for 15 s, 60°C for 30 s and 72°C for 30s. Real-time primer sequences were as follows: GAPDH sense, 5'-CATGGCCTTCCGTGTTCCTA-3' and anti-sense, 5'-ATGCCTGCTTCACCACCTTCT-3'; JHMV nucleocapsid sense, 5'-CGCAGAGTATGGCGACGAT-3' and anti-sense, 5'-GAGGTCCTAGTCTCGGCCTGTT-3'; TNF sense, 5'-GCCACCACGCTCTTCTGTCT-3' and anti-sence, 5'-GGTCTGGGCCATAGAACTGATG-3'; iNOS sense, 5'-GTTCTCAGCCCAACAATACAAGA-3' and anti-sense, 5'-GTGGACGGGTCGATGTCAC-3'; IL-6 sense, 5'-ACACATGTTCTCTGGGAAATCGT-3' and anti-sense, 5'-AAGTGCATCATCGTTGTTCATACA-3'; IL-10 sense, 5'-TTTGAATTCCCTGGGTGAGAA-3' and anti-sense, 5'-GCTCCACTGCCTTGCTCTTATT-3'; TGF-β1 sense, 5'-CCCGAAGCGGACTACTATGC-3' and anti-sense, 5'-CGAATGTCTGACGTATTGAAGAACA-3' ; TAP-1 sense, 5'-CGAGTGTCTCGGGAATGCTG-3' and anti-sense, 5'-GTGAACTGAAGCTGGTAGAGAACGA-3'; MHC class I sense 5'-GCCTCCTCCGTCCACTGA-3' and anti-sense, 5'-GCCACCACAGCTCCAATGAT-3'; CXCL9 sense, 5'-TGCACGATGCTCCTGCA-3' and anti-sense, 5'-AGGTCTTTGAGGGATTTGTAGTGG-3'; CCL2 sense, 5'-AGCAGGTGTCCCAAAGAA-3' and anti-sense, 5'-TATGTCTGGACCCATTCCTT-3'; and CXCL10 sense5'-GACGGTCCGCTGCAACTG-3' and anti-sense 5'-GCTTCCCTATGGCCCTCATT-3'. IFN-γ, IL-17, Suppressor of Cytokine Signaling 1 (SOCS-1) and SOCS-3 mRNA levels were determined using Applied Biosystems Gene Expression Arrays with Universal Taqman Fast Master Mix (Applied Biosystems) in duplicate. PCR conditions were 20 s at 95°C followed by 40 cycles at 95°C for 3 s and 60°C for 30 s. Transcript levels were calculated relative to the housekeeping gene GAPDH using the following formula: $2^{[CT(GAPDH) - CT(Target\ Gene)]} \times 1000$, where CT is determined as the threshold cycle at which the fluorescent signal becomes significantly higher than that of the background. Standard PCR was performed using 2 μl of cDNA and the following primer sequences: JHMV nucleocapsid sense, 5'-GTCGCAAGCCAACAGGCCG-3' and anti-sense, 5'-GGAGTCCTCTTTTGACGAGGC-3'; and hypoxanthine-guanine phosphoribosyltransferase (HPRT) sense, 5'-GTAATGATCAGTCAACGGGGGAC-3' and anti-sense, 5'-CCAGCAAGCTTGCAACCTAACCA-3'. PCR amplification conditions for nucleocapsid consisted of 15 min at 95°C followed by 35 cycles at 95°C for 1 min, 64°C for

1 min, and 72°C for 1min while for GAPDH 15 min at 95°C was followed by 25 cycles at 95°C for 1 min, 60°C for 1 min, and 72°C for 1min.

Statistical analysis

Results are expressed as the mean ± SEM for each group of mice. In all cases, $p < 0.05$ was considered significant. Graphs were plotted and statistics assessed using GraphPad Prism 3.0 software.

Results

B7-H1 protects from encephalitis despite delaying virus control

Greater than 50% of B7-H1$^{-/-}$ mice succumbed to JHMV infection between days 10 and 14 post infection (p.i.), whereas the survival rate in infected wt mice was 80% (Fig. 1*A*). Liver can be a target tissue of JHMV infection in immuno-deficient hosts, potentially contributing to lethality. However, no evidence of acute hepatitis or viral mRNA was detected in the liver of infected B7-H1$^{-/-}$ mice at day 7 p.i. (data not shown). Despite enhanced clinical disease prior to day 12 p.i. (10), surviving B7-H1$^{-/-}$ mice showed more rapid recovery compared to the wt group (Fig. 1*B*). These data suggest that B7-H1 contributes to minimizing morbidity during acute viral encephalitis, but subsequently delays recovery.

Infectious virus in the CNS of both groups was similar at day 5 p.i. indicating no apparent differences in innate antiviral function. However, virus replication was controlled more rapidly in B7-H1$^{-/-}$ mice, approaching the detection threshold by day 10 p.i., whereas all wt mice still harbored infectious virus at this time point (Fig. 1*C*). Quantification of virus infected cells in spinal cords showed an average of 3.4 ± 1.5 infected cells/mm^2 in B7-H1$^{-/-}$ mice compared to 16.5 ± 7.8 infected cells/mm^2 in wt mice at day 10 p.i. In both groups the majority of virus infected cells exhibited a morphology consistent with oligodendrocytes. To confirm that virus primarily infects oligodendrocytes spinal cords from infected syngeneic wt mice expressing GFP under the oligodendrocyte specific proteolipid protein promoter were used to isolate oligodendrocytes and microglia by FACS (43). At day 7 and 10 p.i. viral mRNA encoding the nucleocapsid protein was 19- and 16-fold higher in oligodendrocytes compared to microglia. These results confirm B7-H1 hinders control of infectious virus, as previously suggested by mRNA analysis (10). Notably, accelerated reduction of infectious virus in the absence of B7-H1 coincided with lower levels of persisting viral mRNA in the CNS of survivors (Fig. 2). Thus viral persistence was not prevented by more rapid control of infectious virus during acute infection.

Reduction of virus between days 7 and 10 p.i. correlated with maximal lymphocyte accumulation within the CNS (37). Significantly enhanced antiviral activity in the absence of B7-H1 in both brain and spinal cord thus implied enhanced T cell effector function as the prominent antiviral mechanism. All virus-susceptible glia cell types within the CNS upregulate MHC class I during infection, while only microglia upregulate MHC class II (43, 50). Thus, CD8 T cell effector functions were considered prime candidates in mediating both enhanced viral clearance and morbidity. The consequences of B7-H1 deficiency were investigated in mice infected with a non-pathogenic JHMV derivative containing a deletion in the dominant H-2^b restricted CD8 T cell epitope. This virus variant, designated V2.2/7.2-2, replicates to similar levels within the CNS as the V2.2-1 variant, but does not cause clinical disease or demyelination in wt mice (35, 44). B7-H1$^{-/-}$ mice controlled V2.2/7.2-2 with kinetics similar to wt mice and also remained asymptomatic (data not shown), supporting the notion that increased CD8 T cell effector function leads to enhanced morbidity and mortality in V2.2-1 infected B7-H1$^{-/-}$ mice.

Expansion and recruitment of virus-specific CD8 T cells is independent of B7-H1

T cell responses to JHMV infection are initiated in the draining CLN (51). Although the cell types involved in activating JHMV-specific T cells have not been characterized, expression of B7-H1 by dendritic cells (14) may limit initial T cell activation and expansion. However, no significant differences in the percentages of virus-specific CD8 T cells were detected in the CLN of wt and B7-H1$^{-/-}$ mice between days 5 and 10 p.i. (Fig. 3*A*). Moreover, comparable frequencies of CD62L^{lo} virus-specific CD8 T cells indicated no differences in overall activation. In addition, the frequency of CD62L^{lo} CD4 T cells as well as the kinetics and magnitude of anti-JHMV Ab were not altered by the absence of B7-H1 (Fig. 3*B* and *C*).

To evaluate whether B7-H1 affected CNS accumulation of inflammatory cells or specific subsets, CNS-derived cells were analyzed by flow cytometry. Total numbers of cells recovered from infected wt and B7-H1$^{-/-}$ mice were similar (Table I). Percentages of bone marrow-derived CD45^{hi} CNS-infiltrating cells, as well as their relative proportions of F4/80^{+} monocytes, CD8 T cells, and CD4 T cells were also not significantly altered in B7-H1$^{-/-}$ compared to wt mice (Table I). However the number of total CD8 T cells were consistently elevated in B7-H1$^{-/-}$ mice. Lower percentages of tetramer^{+} cells within the CNS CD8 T cell population in infected B7-H1$^{-/-}$ (Fig. 4*A*) therefore only resulted in reduced numbers of total virus-specific CD8 T cells at day 7 p.i. the peak of T cell infiltration (Fig. 4*B*). Furthermore, CNS-derived B7-H1$^{-/-}$ CD8 T cells, particularly the tetramer negative subset, expressed higher levels of PD-1 compared to wt CD8 T cells (Fig. 4*A*). PD-1 expression was also higher on CNS-infiltrating CD4 T cells (data not shown). These data indicate that neither CD8 T cell expansion, recruitment nor the overall inflammatory cell composition was considerably modified by the absence of B7-H1. Accelerated viral clearance could thus not be attributed to more prominent peripheral expansion or accumulation of virus-specific CD8 T cells within the CNS.

B7-H1 regulates CNS antiviral T cell effector function

PD-1:B7-H1 interactions decrease T cell-mediated IFN-γ secretion (11, 13, 19, 21) as well as cytolytic function *in vitro* (11, 24). Enhanced viral control in the absence of B7-H1 thus predicted increased T cell activity at a cellular level. Virus-specific CD8 T cells from infected B7-H1$^{-/-}$ mice assayed directly *ex vivo* without peptide stimulation expressed higher levels of granzyme B compared to those derived from CNS of wt mice at day 7 p.i., consistent with increased *in vivo* effector function (Fig. 5*A*). Granzyme expression was even further increased by day 10 p.i. By contrast, granzyme B in the tetramer negative populations remained similar between both groups, indicating enhanced effector function is specific to viral Ag. Furthermore, although CD4 T cells have the potential to be cytolytic, granzyme B was only detected in a minor fraction of CD4 T cells, and the relatively small expression levels were not significantly influenced by the absence of B7-H1 (Fig. 5*B*).

IFN-γ not only increases MHC class I expression on glial cells (43, 50) but also controls JHMV infection of oligodendroglia (38-40). IFN-γ levels within the CNS were low at day 5 p.i., peaked by day 7 p.i., and subsequently declined by day 10 p.i. in both groups demonstrating similar kinetics of IFN-γ expression following infection (Fig. 5*C*). Despite similar kinetics, IFN-γ levels were significantly higher in the CNS of B7-H1$^{-/-}$ mice at days 7 and 10 p.i., confirming increased *in vivo* effector function. IFN-γ mRNA was also increased ~2-fold relative to wt mice at day 7 p.i. (data not shown), supporting TCR driven transcriptional regulation (52). As viral Ag and mRNA are most abundant in oligodendrocytes, which upregulate MHC class I but not MHC class II during infection (43), we tested whether CD8 T cells contributed most prominently towards increased IFN-γ production. To circumvent *in vitro* manipulation introduced by peptide stimulation and external target cells, T cell subsets were directly FACS purified from the infected CNS at

day 7 p.i. and subjected to mRNA analysis (Table II). Levels of IFN-γ mRNA were indeed ~1.6-fold higher in tetramer^{+} CD8 T cells from B7-H1$^{-/-}$ mice relative to wt mice. Furthermore, the tetramer^{-} CD8 T cell populations from both groups contained only 15-20 % the IFN-γ mRNA levels detected in the tetramer^{+} cells, confirming a minor contribution to overall IFN-γ levels. Surprisingly, purified CD4 T cells from wt mice harbored ~2-fold higher IFN-γ mRNA than virus-specific CD8 T cells. Moreover, CD4 T cells from B7-H1$^{-/-}$ mice also expressed higher IFN-γ mRNA levels relative to their wt counterparts, similar to CD8 T cells. Increased IFN-γ expression by CD4 T cells relative to CD8 T cells was thus sustained in B7-H1$^{-/-}$ mice. Analysis of TNF mRNA as an alternate indicator of T cell activity suggested enhanced expression is only observed in tetramer^{+} CD8 T cells in B7-H1$^{-/-}$ mice, but that expression is overall low relative to wt CD4 T cells. Furthermore, IL-17 mRNA remains barely detectable in T cells from both groups, suggesting no contribution of T cell derived IL-17 to increased morbidity. These results thus indicate that both CD8 and CD4 T cells contribute to elevated IFN-γ within the CNS. Overall, these data support the notion that enhanced clearance of infectious virus from the CNS of B7-H1$^{-/-}$ mice is a direct consequence of elevated IFN-γ and granzyme B production at the cellular level.

B7-H1 ameliorates axonal loss

Primary demyelination with relative sparing of axons is a hallmark of JHMV infection (45, 53) and the focal areas of myelin loss are tightly linked to T cell-mediated effector functions (41, 54-56). Surprisingly, although myelin producing oligodendrocytes are the major targets of infection, B7-H1 expression did not affect the overall size, number or distribution of focal lesions of myelin loss following JHMV infection during acute disease (Fig. 6) (data not shown) (10) or in B7-H1$^{-/-}$ survivors at 31 days p.i. (data not shown). Quantitative analysis revealed approximately 2% of spinal cord area was demyelinated at day 10 p.i. in both groups. Oligodendrocytes within the area of myelin loss were counted using anti-APC (40) to determine if the increased control of infectious virus correlated with alterations in oligodendrocyte loss. APC positive cells decreased between days 7 and 10 p.i. within the areas of myelin loss in both groups; however, there was no evidence for enhanced oligodendrocyte loss either within the lesions or in normal white matter in B7-H1$^{-/-}$ spinal cords (data not shown). Although B7-H1 did not affect the area of myelin loss (Fig. 6) or the numbers of oligodendrocytes, areas within each lesion exhibited increased demyelination and axonal damage. Axonal integrity was assessed by dual staining with mAb SMI-31, specific for phosphorylated neurofilaments, and mAb SMI-32, specific for nonphosphorylated neurofilaments. Axonal damage was confined to areas within the demyelinated lesions in both groups (Fig. 6) but was enhanced within the lesions in infected B7-H1$^{-/-}$ mice (Fig. 6). As rare infected neurons are cleared of virus prior to T cell infiltration (45, 57), these results suggest that the prominent B7-H1 expression on oligodendocytes reduces bystander tissue destruction in contrast to dampening direct cytolysis of oligodendrocytes. Increased mortality thus coincides with enhanced axonal damage.

No evidence for enhanced neuronal infection in B7-H1$^{-/-}$ mice implied that the mechanisms underlying axonal bystander damage may be due to misdirected T cell effector activity or to secondary effects. Exaggerated T cell effector function within the CNS of B7-H1$^{-/-}$mice suggested a possible contribution of increased apoptosis to enhanced tissue destruction. The vast majority of apoptotic cells in the CNS during JHMV infection are lymphocytes (40, 58) with only rare apoptotic oligodendrocytes (59). No evidence for neuronal apoptosis was detected in either group and the absence of B7-H1 expression coincided with only a slight elevation in apoptotic cells within the areas of myelin loss (Fig. 7); however, in both wt and B7-H1$^{-/-}$ mice their morphology was consistent with lymphocytes (40, 58). The areas of myelin loss were examined for T cells and macrophages/microglia to determine the cellular

composition associated with increased tissue destruction. Compared to the few T cells within the lesions of wt mice, lesions in B7-H1$^{-/-}$ mice contained increased numbers of T cells, which appeared more clustered relative to the random distribution in wt mice (Fig. 7). In addition to increased T cells within the lesions, macrophage/microglia exhibited increased cytoplasmic content and a less ramified phenotype (Fig. 7), consistent with enhanced activation of microglia/macrophages by elevated IFN-γ (41, 60, 61). The data further support an association between increased IFN-γ and enhanced clinical disease without affecting demyelination noted previously during JHMV infection (46).

B7-H1 dampens pro-inflammatory cytokines but not chemokines

Numerous pro-inflammatory mediators exacerbate CNS disease during infection and autoimmunity (60, 62-66). TNF and iNOS are common markers of activation and potential mediators of neurotoxicity (60, 67). TNF and iNOS mRNA expression in the CNS were similar in both groups at day 7 p.i. (Fig. 8). However, in contrast to the decline of iNOS and TNF mRNA in wt mice by day 10 p.i., mRNA levels were maintained in B7-H1$^{-/-}$ mice, consistent with elevated IFN-γ (see Fig. 5*C*). Notably, IL-17 mRNA levels were similarly low in the CNS of infected wt and B7-H1$^{-/-}$ mice (Fig. 8), confirming results from purified T cells (Table II) and excluding a role of IL-17 in this model (46). Furthermore, CCL2, CXCL9 and CXCL10 mRNA levels were comparable in the CNS of both groups (Fig. 8), consistent with similar overall cell recruitment in the absence of B7-H1 (Table I). Lastly, a similar decline in IL-6 mRNA expression in both groups by day 10 p.i. confirmed no differences in ongoing innate signaling (Fig. 8).

The more activated morphology of microglia/macrophages in lesions of B7-H1$^{-/-}$ mice suggested these populations may contribute to sustained iNOS and TNF mRNA expression. CD45^{lo} microglia and infiltrating CD45^{hi}CD11b^{+} monocyte-derived macrophages were therefore purified from the CNS of infected wt and B7-H1$^{-/-}$ mice at 10 days p.i. to assess their contributions to expression of potentially toxic mediators. Expression of iNOS mRNA was considerably higher in infiltrating monocyte-derived macrophages versus microglia in both groups regardless of their derivation from brain or spinal cord (Fig. 9). Furthermore, both microglia and infiltrating monocyte-derived macrophages from B7-H1$^{-/-}$ infected mice expressed elevated iNOS mRNA. In the brain, iNOS expression by B7-H1$^{-/-}$ derived microglia and macrophages was increased 6.3 ± 2.2 and 5.2 ± 0.7 fold, respectively, while levels in spinal cord were enhanced by 2.2 ± 0.1 and 2.7 ± 0.6 fold relative to their wt counterparts. TNF mRNA levels were also elevated in B7-H1$^{-/-}$ microglia relative to wt microglia (Fig. 9) with modest 1.9 ± 0.1 and 2.0 ± 0.1 fold increases in the brain and spinal cord, respectively. No differences in TNF mRNA expression were detected comparing wt and B7-H1$^{-/-}$ derived infiltrating monocyte-derived macrophages. Although elevated iNOS mRNA reflected enhanced and sustained IFN-γ expression, IFN inducible mRNA transcripts for MHC class I and TAP-1 remained similar (Fig. 9). These data indicated that increased and prolonged T cell effector function in infected B7-H1$^{-/-}$ mice is associated with sustained microglia and macrophage activation, iNOS and TNF expression, potentially contributing to enhanced morbidity and mortality.

Anti-inflammatory responses within the CNS of B7-H1$^{-/-}$ mice are insufficient to counteract morbidity

In addition to tempering T cell function, B7-H1-mediated signaling may be required for conversion of naive CD4 T cells to adaptive regulatory T cells (Tregs) by dendritic cells (36). Tregs are protective during lethal JHMV infection (68). Therefore, we tested whether recruitment of CD4^{+}Foxp3^{+} Tregs into the CNS was impaired in the absence of B7-H1. Modestly elevated percentages of Foxp3^{+} T cells were found in the CLN of B7-H1$^{-/-}$ mice compared to wt mice (data not shown). The percentage of Foxp3^{+} T cells was also slightly

higher in the CNS of B7-H1$^{-/-}$ mice at day 7 p.i. compared to wt mice and equivalent by day 10 p.i. (Fig. 10*A*). Impaired activation or recruitment of Treg is thus unlikely to contribute to increased mortality and T cell activity in B7-H1$^{-/-}$ mice. To further verify that expression of the anti-inflammatory response within the CNS is not negatively affected by B7-H1 deficiency, mRNAs specific for TGF-β1, IL-10, SOCS-1 and SOCS-3 were measured. TGF-β1 mRNA levels were similar in both groups at days 7 and 10 p.i. and did not decline within this timeframe (Fig. 10*B*). While IL-10 plays a protective role in JHMV induced morbidity and mortality (69), the role of SOCS-1 and SOCS-3, IFN-γ inducible inhibitors of cytokine signaling pathways (70), has not been explored. All three transcript levels were significantly elevated at day 7 p.i. in both infected groups compared to naive mice (Fig. 10). IL-10 and SOCS-3 mRNA levels were significantly higher in the CNS of B7-H1$^{-/-}$ versus wt mice at day 7 p.i. (Fig. 10*C* and *D*) and declined by day 10 p.i. in both groups. However, expression remained elevated in the absence of B7-H1. IL-10 protein levels in the CNS were also higher in B7-H1$^{-/-}$ compared to wt mice at day 7 p.i. (data not shown). SOCS-1 mRNA expression did not differ between B7-H1$^{-/-}$ versus wt mice (Fig. 10*E*), indicating distinct regulation of these SOCS genes. Similar Treg accumulation and no evident impairment in anti-inflammatory responses in B7-H1$^{-/-}$ mice suggested that these otherwise protective mediators induced during CNS inflammation were insufficient to counteract the increased severity of the white matter lesions and clinical disease.

Discussion

The modulating effects of PD-1:B7-H1 interactions on virus-induced encephalitis, viral control, and persistence within the CNS have not been studied extensively. The present study analyzed cellular mechanisms underlying enhanced virus control, the consequences on CNS viral persistence and immunopathology in B7-H1$^{-/-}$ mice infected with a neurotropic conronavirus. B7-H1 did not alter peripheral expansion of virus-specific CD8 T cells or overall accumulation of CNS-infiltrating cells; however, the percentages of virus-specific CD8 T cells within the CNS were consistently reduced in B7-H1$^{-/-}$ mice. The increased tetramer negative CD8 T cells within the CNS may arise from an increased T cell receptor repertoire, similar to T cells in the CNS of PD-1$^{-/-}$ mice during EAE (71) and/or preferential apoptosis of virus-specific T cells due to enhanced activation. Increased mortality and focal tissue destruction were thus directly attributed to altered T cell:target interactions locally within the CNS, rather than increased T cell activation in lymphoid tissue observed during non-microbial driven models of CNS disease in B7-H1$^{-/-}$ mice (72, 73).

CD8 T cells play a dominant role in controlling JHMV replication via both cytolytic activity and IFN-γ (38-41). Nevertheless, both CD8 and CD4 T cells contribute to viral pathogenesis (34, 54-56), unlike predominant CD4 or CD8 T cell driven pathology during EAE or transgene driven CNS inflammation, respectively (74, 75). More rapid control of virus replication in oligodendrocytes, which express MHC class I, but not MHC class II, directly implicated CD8 T cell activities as primary antiviral mediators, as well as candidates for causing exacerbated disease. This notion was supported by the similar kinetics of virus clearance from the CNS of B7-H1$^{-/-}$ and wt mice infected with a JHMV variant lacking the dominant CD8 T cell epitope. B7-H1 deficiency indeed coincided with significantly enhanced granzyme B expression specifically in virus-specific CD8 T cells. Similarly, IFN-γ mRNA levels were increased in virus-specific CD8 T cells derived from the CNS of B7-H1$^{-/-}$ mice, supporting increased effector function. However, CD4 T cells also contained increased IFN-γ mRNA levels clearly indicating that CD4 T cells make a prominent contribution to overall increased IFN-γ protein levels in the CNS of B7-H1$^{-/-}$ mice. This finding was surprising as MHC class II expressing microglia/monocytes are more sparsely infected compared to oligodendrocytes. Whether CD4 T cell activation in the CNS results from cross-presentation in addition to direct engagement of infected cells and how B7-H1

affects this interaction remains to be determined. While our data are thus consistent with increased T cell activity in the CNS of B7-H1$^{-/-}$ mice with EAE, they differ in that enhanced activation was evident at the cellular level rather than the increased population of IFN-γ producing T cells during EAE (73). Although increased T cell effector function was reflected in more efficient virus control in B7-H1$^{-/-}$ mice, ongoing detection of persisting viral mRNA demonstrated that accelerated viral control alone cannot prevent viral persistence. Furthermore, similar antiviral Ab responses following infection support a negligible role of B7-H1 in modulating humoral immunity, consistent with the Ab responses in B7-H1$^{-/-}$and wt mice following immunization with myelin oligodendrocyte glycoprotein (71).

Similar to viral infection of neurons (76-78), IFN-γ is crucial in non-cytolytic control of JHMV infection in oligodendrocytes, which appear resistant to perforin/granzyme-mediated cytolysis in wt mice (40, 79). Surprisingly, even the absence of B7-H1 on oligodendrocytes did not enhance vulnerability to CD8 T cell cytolysis, as indicated by similar extent of myelin loss (10), similar morphology of apoptotic cells, and the absence of increased oligodendrocyte loss. In contrast to rabies virus infection (6), we found no evidence supporting a contribution of B7-H1 to apoptosis of effector T cells. Elevated numbers of T cells coincided with a modest increase in apoptotic cells only within lesions of B7-H1$^{-/-}$ mice, suggesting a focal interaction between T cells with infected cells resulting in activation within the white matter.

Despite a similar extent of myelin loss increased T cell effector function in B7-H1$^{-/-}$ mice coincided with more severe damage within the lesions, characterized by extensive axonal damage as well as increased microglia/macrophage activation. Although CD8 T cells are likely candidates contributing to greater axonal injury in infected B7-H1$^{-/-}$ mice, it remains unclear whether injury results from direct release of antiviral mediators or from participation of toxic factors released by activated macrophages. Increased axonal loss is also a hallmark of PD-1 deficient myelin mutant mice with EAE (71), presumably mediated by activated CD4 T cells. However, participation of CD8 T cells in triggering axonal damage has been demonstrated in Theiler's murine encephalomyelitis virus infection (80) as well as in *in vitro* (81). However, unlike MHC class I dependent CD8 T cell-mediated axonal injury in the latter model, rare infection of neurons by glia-tropic JHMV argues against direct axonal damage by CD8 T cells. Extensive *in vivo* bystander killing of neurons as a consequence of cytotoxic CD8 T cell attack on surrounding astrocytes (82) and axonal loss resulting from bystander damage by auto-aggressive, myelin-directed cytotoxic CD8 T cells (83) both favor T cell-mediated bystander damage as the cause of increased axonal injury.

Sustained mRNA expression of the neurotoxic pro-inflammatory mediators TNF and iNOS, coincident with increased activation of the microglia/macrophage population within demyelinated lesions in B7-H1$^{-/-}$ mice, suggested dysregulation of these cells may also contribute to the increase in axonal damage. Although both iNOS and TNF play negligible roles in JHMV pathogenesis (84, 85), it cannot be ruled out that elevated expression of neurotoxic factors by infiltrating monocyte-derived macrophages in B7-H1$^{-/-}$ mice may have deleterious local effects, specifically proximal to neurons. Similarly, prolonged expression of TNF by B7-H1$^{-/-}$ microglia may increase cytotoxicity and/or decrease neuroprotective functions. Notably, elevated expression of IFN-γ, TNF and iNOS mRNA also coincides with exacerbated disease in JHMV infected IL-10$^{-/-}$ mice (69). In this context it is also of interest that SOCS-3 is essential for the function of classically activated M1 macrophages (86). Enhanced IFN-γ induced SOCS-3 in the absence of B7-H1 may thus promote an M1 phenotype in CNS macrophages, enhancing tissue damage rather than dampening the pro-inflammatory response. Increased expression of pro-inflammatory molecules and tissue

damage was paralleled by elevated IL-10 indicating this anti-inflammatory mediator was clearly insufficient to counteract enhanced T cell and microglia/ macrophage activation.

In summary, our data demonstrate that B7-H1 down-regulation of T cell effector function delays control of virus replication in the CNS, contributes to viral persistence and is vital in containing bystander damage to non-infected cells. These results are consistent with studies suggesting a protective role of B7-H1 in limiting damage to bystander cells via regulation of T cell activity. However, expression of B7-H1 by the respective target cells was not analyzed. Our studies demonstrate that B7-H1 expression on oligodendrocytes, the major targets of infection, impedes virus clearance without preventing CD8 T cell-mediated cytolysis. However, by tempering CD8 T cell-mediated activity, B7-H1 may not only prevent damage to uninfected bystander cells, but indirectly protect from sustained activation and release of neurotoxic factors by infiltrating monocyte-derived macrophages and microglia. Elimination of these protective functions to accelerate control of viral infection is thus severely compromised by enhanced focal tissue damage and increased morbidity.

Acknowledgments

We sincerely thank Wenqiang Wei for exceptional technical assistance and Parul Kapil for providing PCR results from sorted oligodendroglia.

References

1. Keir ME, Butte MJ, Freeman GJ, Sharpe AH. PD-1 and its ligands in tolerance and immunity. Annu Rev Immunol. 2008; 26:677–704. [PubMed: 18173375]
2. Agata Y, Kawasaki A, Nishimura H, Ishida Y, Tsubata T, Yagita H, Honjo T. Expression of the PD-1 antigen on the surface of stimulated mouse T and B lymphocytes. Int Immunol. 1996; 8:765–772. [PubMed: 8671665]
3. Golden-Mason L, Klarquist J, Wahed AS, Rosen HR. Cutting edge: programmed death-1 expression is increased on immunocytes in chronic hepatitis C virus and predicts failure of response to antiviral therapy: race-dependent differences. J Immunol. 2008; 180:3637–3641. [PubMed: 18322167]
4. Huang X, Venet F, Wang YL, Lepape A, Yuan Z, Chen Y, Swan R, Kherouf H, Monneret G, Chung CS, Ayala A. PD-1 expression by macrophages plays a pathologic role in altering microbial clearance and the innate inflammatory response to sepsis. Proc Natl Acad Sci U S A. 2009; 106:6303–6308. [PubMed: 19332785]
5. Petrovas C, Casazza JP, Brenchley JM, Price DA, Gostick E, Adams WC, Precopio ML, Schacker T, Roederer M, Douek DC, Koup RA. PD-1 is a regulator of virus-specific CD8+ T cell survival in HIV infection. J Exp Med. 2006; 203:2281–2292. [PubMed: 16954372]
6. Lafon M, Megret F, Meuth SG, Simon O, Velandia Romero ML, Lafage M, Chen L, Alexopoulou L, Flavell RA, Prehaud C, Wiendl H. Detrimental contribution of the immuno-inhibitor B7-H1 to rabies virus encephalitis. J Immunol. 2008; 180:7506–7515. [PubMed: 18490751]
7. Lipp M, Brandt C, Dehghani F, Kwidzinski E, Bechmann I. PD-L1 (B7-H1) regulation in zones of axonal degeneration. Neurosci Lett. 2007; 425:156–161. [PubMed: 17825988]
8. Magnus T, Schreiner B, Korn T, Jack C, Guo H, Antel J, Ifergan I, Chen L, Bischof F, Bar-Or A, Wiendl H. Microglial expression of the B7 family member B7 homolog 1 confers strong immune inhibition: implications for immune responses and autoimmunity in the CNS. J Neurosci. 2005; 25:2537–2546. [PubMed: 15758163]
9. Maier H, Isogawa M, Freeman GJ, Chisari FV. PD-1:PD-L1 interactions contribute to the functional suppression of virus-specific CD8+ T lymphocytes in the liver. J Immunol. 2007; 178:2714–2720. [PubMed: 17312113]
10. Phares TW, Ramakrishna C, Parra GI, Epstein A, Chen L, Atkinson R, Stohlman SA, Bergmann CC. Target-dependent B7-H1 regulation contributes to clearance of central nervous system infection and dampens morbidity. J Immunol. 2009; 182:5430–5438. [PubMed: 19380790]

11. Rodig N, Ryan T, Allen JA, Pang H, Grabie N, Chernova T, Greenfield EA, Liang SC, Sharpe AH, Lichtman AH, Freeman GJ. Endothelial expression of PD-L1 and PD-L2 down-regulates CD8+ T cell activation and cytolysis. Eur J Immunol. 2003; 33:3117–3126. [PubMed: 14579280]
12. Salama AD, Chitnis T, Imitola J, Ansari MJ, Akiba H, Tushima F, Azuma M, Yagita H, Sayegh MH, Khoury SJ. Critical role of the programmed death-1 (PD-1) pathway in regulation of experimental autoimmune encephalomyelitis. J Exp Med. 2003; 198:71–78. [PubMed: 12847138]
13. Usui Y, Okunuki Y, Hattori T, Kezuka T, Keino H, Ebihara N, Sugita S, Usui M, Goto H, Takeuchi M. Functional expression of B7H1 on retinal pigment epithelial cells. Exp Eye Res. 2008; 86:52–59. [PubMed: 17981268]
14. Yamazaki T, Akiba H, Iwai H, Matsuda H, Aoki M, Tanno Y, Shin T, Tsuchiya H, Pardoll DM, Okumura K, Azuma M, Yagita H. Expression of programmed death 1 ligands by murine T cells and APC. J Immunol. 2002; 169:5538–5545. [PubMed: 12421930]
15. Schreiner B, Mitsdoerffer M, Kieseier BC, Chen L, Hartung HP, Weller M, Wiendl H. Interferon-beta enhances monocyte and dendritic cell expression of B7-H1 (PD-L1), a strong inhibitor of autologous T-cell activation: relevance for the immune modulatory effect in multiple sclerosis. J Neuroimmunol. 2004; 155:172–182. [PubMed: 15342209]
16. Benedict CA, Loewendorf A, Garcia Z, Blazar BR, Janssen EM. Dendritic cell programming by cytomegalovirus stunts naive T cell responses via the PD-L1/PD-1 pathway. J Immunol. 2008; 180:4836–4847. [PubMed: 18354207]
17. Day CL, Kaufmann DE, Kiepiela P, Brown JA, Moodley ES, Reddy S, Mackey EW, Miller JD, Leslie AJ, DePierres C, Mncube Z, Duraiswamy J, Zhu B, Eichbaum Q, Altfeld M, Wherry EJ, Coovadia HM, Goulder PJ, Klenerman P, Ahmed R, Freeman GJ, Walker BD. PD-1 expression on HIV-specific T cells is associated with T-cell exhaustion and disease progression. Nature. 2006; 443:350–354. [PubMed: 16921384]
18. Iwai Y, Terawaki S, Ikegawa M, Okazaki T, Honjo T. PD-1 inhibits antiviral immunity at the effector phase in the liver. J Exp Med. 2003; 198:39–50. [PubMed: 12847136]
19. Jeong HY, Lee YJ, Seo SK, Lee SW, Park SJ, Lee JN, Sohn HS, Yao S, Chen L, Choi I. Blocking of monocyte-associated B7-H1 (CD274) enhances HCV-specific T cell immunity in chronic hepatitis C infection. J Leukoc Biol. 2008; 83:755–764. [PubMed: 18086898]
20. Sester U, Presser D, Dirks J, Gartner BC, Kohler H, Sester M. PD-1 expression and IL-2 loss of cytomegalovirus- specific T cells correlates with viremia and reversible functional anergy. Am J Transplant. 2008; 8:1486–1497. [PubMed: 18510628]
21. Trautmann L, Janbazian L, Chomont N, Said EA, Gimmig S, Bessette B, Boulassel MR, Delwart E, Sepulveda H, Balderas RS, Routy JP, Haddad EK, Sekaly RP. Upregulation of PD-1 expression on HIV-specific CD8+ T cells leads to reversible immune dysfunction. Nat Med. 2006; 12:1198–1202. [PubMed: 16917489]
22. Wherry EJ, Blattman JN, Murali-Krishna K, van der Most R, Ahmed R. Viral persistence alters CD8 T-cell immunodominance and tissue distribution and results in distinct stages of functional impairment. J Virol. 2003; 77:4911–4927. [PubMed: 12663797]
23. Wherry EJ, Ha SJ, Kaech SM, Haining WN, Sarkar S, Kalia V, Subramaniam S, Blattman JN, Barber DL, Ahmed R. Molecular signature of CD8+ T cell exhaustion during chronic viral infection. Immunity. 2007; 27:670–684. [PubMed: 17950003]
24. Wong RM, Scotland RR, Lau RL, Wang C, Korman AJ, Kast WM, Weber JS. Programmed death-1 blockade enhances expansion and functional capacity of human melanoma antigen-specific CTLs. Int Immunol. 2007; 19:1223–1234. [PubMed: 17898045]
25. Zajac AJ, Blattman JN, Murali-Krishna K, Sourdive DJ, Suresh M, Altman JD, Ahmed R. Viral immune evasion due to persistence of activated T cells without effector function. J Exp Med. 1998; 188:2205–2213. [PubMed: 9858507]
26. Carter LL, Leach MW, Azoitei ML, Cui J, Pelker JW, Jussif J, Benoit S, Ireland G, Luxenberg D, Askew GR, Milarski KL, Groves C, Brown T, Carito BA, Percival K, Carreno BM, Collins M, Marusic S. PD-1/PD-L1, but not PD-1/PD-L2, interactions regulate the severity of experimental autoimmune encephalomyelitis. J Neuroimmunol. 2007; 182:124–134. [PubMed: 17182110]

27. Grabie N, Gotsman I, DaCosta R, Pang H, Stavrakis G, Butte MJ, Keir ME, Freeman GJ, Sharpe AH, Lichtman AH. Endothelial programmed death-1 ligand 1 (PD-L1) regulates CD8+ T-cell mediated injury in the heart. Circulation. 2007; 116:2062–2071. [PubMed: 17938288]
28. Jun H, Seo SK, Jeong HY, Seo HM, Zhu G, Chen L, Choi IH. B7-H1 (CD274) inhibits the development of herpetic stromal keratitis (HSK). FEBS Lett. 2005; 579:6259–6264. [PubMed: 16253242]
29. Peng G, Li S, Wu W, Tan X, Chen Y, Chen Z. PD-1 upregulation is associated with HBV-specific T cell dysfunction in chronic hepatitis B patients. Mol Immunol. 2008; 45:963–970. [PubMed: 17868872]
30. Onlamoon N, Rogers K, Mayne AE, Pattanapanyasat K, Mori K, Villinger F, Ansari AA. Soluble PD-1 rescues the proliferative response of simian immunodeficiency virus-specific CD4 and CD8 T cells during chronic infection. Immunology. 2008; 124:277–293. [PubMed: 18266718]
31. Penna A, Pilli M, Zerbini A, Orlandini A, Mezzadri S, Sacchelli L, Missale G, Ferrari C. Dysfunction and functional restoration of HCV-specific CD8 responses in chronic hepatitis C virus infection. Hepatology. 2007; 45:588–601. [PubMed: 17326153]
32. Radziewicz H, Ibegbu CC, Fernandez ML, Workowski KA, Obideen K, Wehbi M, Hanson HL, Steinberg JP, Masopust D, Wherry EJ, Altman JD, Rouse BT, Freeman GJ, Ahmed R, Grakoui A. Liver-infiltrating lymphocytes in chronic human hepatitis C virus infection display an exhausted phenotype with high levels of PD-1 and low levels of CD127 expression. J Virol. 2007; 81:2545–2553. [PubMed: 17182670]
33. Urbani S, Amadei B, Tola D, Massari M, Schivazappa S, Missale G, Ferrari C. PD-1 expression in acute hepatitis C virus (HCV) infection is associated with HCV-specific CD8 exhaustion. J Virol. 2006; 80:11398–11403. [PubMed: 16956940]
34. Bergmann CC, Altman JD, Hinton D, Stohlman SA. Inverted immunodominance and impaired cytolytic function of CD8+ T cells during viral persistence in the central nervous system. J Immunol. 1999; 163:3379–3387. [PubMed: 10477608]
35. Marten NW, Stohlman SA, Bergmann CC. MHV infection of the CNS:mechanisms of immune-mediated control. Viral Immunol. 2001; 14:1–18. [PubMed: 11270593]
36. Wang L, Pino-Lagos K, de Vries VC, Guleria I, Sayegh MH, Noelle RJ. Programmed death 1 ligand signaling regulates the generation of adaptive Foxp3+CD4+ regulatory T cells. Proc Natl Acad Sci U S A. 2008; 105:9331–9336. [PubMed: 18599457]
37. Bergmann CC, Lane TE, Stohlman SA. Coronavirus infection of the central nervous system: host-virus stand-off. Nat Rev Microbiol. 2006; 4:121–132. [PubMed: 16415928]
38. Parra B, Hinton DR, Marten NW, Bergmann CC, Lin MT, Yang CS, Stohlman SA. IFN-gamma is required for viral clearance from central nervous system oligodendroglia. J Immunol. 1999; 162:1641–1647. [PubMed: 9973424]
39. Lin MT, Stohlman SA, Hinton DR. Mouse hepatitis virus is cleared from the central nervous systems of mice lacking perforin-mediated cytolysis. J Virol. 1997; 71:383–391. [PubMed: 8985361]
40. Gonzalez JM, Bergmann CC, Ramakrishna C, Hinton DR, Atkinson R, Hoskin J, Macklin WB, Stohlman SA. Inhibition of interferon-gamma signaling in oligodendroglia delays coronavirus clearance without altering demyelination. Am J Pathol. 2006; 168:796–804. [PubMed: 16507895]
41. Bergmann CC, Parra B, Hinton DR, Ramakrishna C, Dowdell KC, Stohlman SA. Perforin and gamma interferon-mediated control of coronavirus central nervous system infection by CD8 T cells in the absence of CD4 T cells. J Virol. 2004; 78:1739–1750. [PubMed: 14747539]
42. Dong H, Zhu G, Tamada K, Flies DB, van Deursen JM, Chen L. B7-H1 determines accumulation and deletion of intrahepatic CD8(+) T lymphocytes. Immunity. 2004; 20:327–336. [PubMed: 15030776]
43. Malone KE, Stohlman SA, Ramakrishna C, Macklin W, Bergmann CC. Induction of class I antigen processing components in oligodendroglia and microglia during viral encephalomyelitis. Glia. 2008; 56:426–435. [PubMed: 18205173]
44. Fleming JO, Trousdale MD, el-Zaatari FA, Stohlman SA, Weiner LP. Pathogenicity of antigenic variants of murine coronavirus JHM selected with monoclonal antibodies. J Virol. 1986; 58:869–875. [PubMed: 3701929]

45. Ireland DD, Stohlman SA, Hinton DR, Kapil P, Silverman RH, Atkinson RA, Bergmann CC. RNase L mediated protection from virus induced demyelination. PLoS Pathog. 2009; 5:e1000602. [PubMed: 19798426]
46. Kapil P, Atkinson R, Ramakrishna C, Cua DJ, Bergmann CC, Stohlman SA. Interleukin-12 (IL-12), but not IL-23, deficiency ameliorates viral encephalitis without affecting viral control. J Virol. 2009; 83:5978–5986. [PubMed: 19339350]
47. Tschen SI, Bergmann CC, Ramakrishna C, Morales S, Atkinson R, Stohlman SA. Recruitment kinetics and composition of antibody-secreting cells within the central nervous system following viral encephalomyelitis. J Immunol. 2002; 168:2922–2929. [PubMed: 11884463]
48. Tschen SI, Stohlman SA, Ramakrishna C, Hinton DR, Atkinson RD, Bergmann CC. CNS viral infection diverts homing of antibody-secreting cells from lymphoid organs to the CNS. Eur J Immunol. 2006; 36:603–612. [PubMed: 16437540]
49. Ireland DD, Stohlman SA, Hinton DR, Atkinson R, Bergmann CC. Type I interferons are essential in controlling neurotropic coronavirus infection irrespective of functional CD8 T cells. J Virol. 2008; 82:300–310. [PubMed: 17928334]
50. Hamo L, Stohlman SA, Otto-Duessel M, Bergmann CC. Distinct regulation of MHC molecule expression on astrocytes and microglia during viral encephalomyelitis. Glia. 2007; 55:1169–1177. [PubMed: 17600339]
51. Marten NW, Stohlman SA, Zhou J, Bergmann CC. Kinetics of virus-specific CD8+ -T-cell expansion and trafficking following central nervous system infection. J Virol. 2003; 77:2775–2778. [PubMed: 12552021]
52. Slifka MK, Whitton JL. Activated and memory CD8+ T cells can be distinguished by their cytokine profiles and phenotypic markers. J Immunol. 2000; 164:208–216. [PubMed: 10605013]
53. Dandekar AA, Wu GF, Pewe L, Perlman S. Axonal damage is T cell mediated and occurs concomitantly with demyelination in mice infected with a neurotropic coronavirus. J Virol. 2001; 75:6115–6120. [PubMed: 11390613]
54. Lane TE, Liu MT, Chen BP, Asensio VC, Samawi RM, Paoletti AD, Campbell IL, Kunkel SL, Fox HS, Buchmeier MJ. A central role for CD4(+) T cells and RANTES in virus-induced central nervous system inflammation and demyelination. J Virol. 2000; 74:1415–1424. [PubMed: 10627552]
55. Savarin C, Bergmann CC, Hinton DR, Ransohoff RM, Stohlman SA. Memory CD4+ T-cell-mediated protection from lethal coronavirus encephalomyelitis. J Virol. 2008; 82:12432–12440. [PubMed: 18842712]
56. Wu GF, Dandekar AA, Pewe L, Perlman S. CD4 and CD8 T cells have redundant but not identical roles in virus-induced demyelination. J Immunol. 2000; 165:2278–2286. [PubMed: 10925317]
57. Wang F-I, Hinton DR, Gilmore W, Trousdale MD, Fleming JO. Sequential Infection of Glial Cells by the Murine Hepatitis Virus JHM Strain (MHV-4) Leads to a Characteristic Distribution of Demyelination. Lab Invest. 1992; 66:744–754. [PubMed: 1318460]
58. Stohlman SA, Bergmann CC, Cua DJ, Lin MT, Ho S, Wei W, Hinton DR. Apoptosis of JHMV-specific CTL in the CNS in the absence of CD4+ T cells. Adv Exp Med Biol. 1998; 440:425–430. [PubMed: 9782310]
59. Schwartz T, Fu L, Lavi E. Differential induction of apoptosis in demyelinating and nondemyelinating infection by mouse hepatitis virus. J Neurovirol. 2002; 8:392–399. [PubMed: 12402165]
60. Munoz-Fernandez MA, Fresno M. The role of tumour necrosis factor, interleukin 6, interferon-gamma and inducible nitric oxide synthase in the development and pathology of the nervous system. Prog Neurobiol. 1998; 56:307–340. [PubMed: 9770242]
61. Schroder K, Hertzog PJ, Ravasi T, Hume DA. Interferon-gamma: an overview of signals, mechanisms and functions. J Leukoc Biol. 2004; 75:163–189. [PubMed: 14525967]
62. Campbell IL, Samimi A, Chiang CS. Expression of the inducible nitric oxide synthase. Correlation with neuropathology and clinical features in mice with lymphocytic choriomeningitis. J Immunol. 1994; 153:3622–3629. [PubMed: 7523499]

63. Carmen J, Rothstein JD, Kerr DA. Tumor necrosis factor-alpha modulates glutamate transport in the CNS and is a critical determinant of outcome from viral encephalomyelitis. Brain Res. 2009; 1263:143–154. [PubMed: 19368827]
64. Martin D, Near SL, Bendele A, Russell DA. Inhibition of tumor necrosis factor is protective against neurologic dysfunction after active immunization of Lewis rats with myelin basic protein. Exp Neurol. 1995; 131:221–228. [PubMed: 7534720]
65. Okuda Y, Nakatsuji Y, Fujimura H, Esumi H, Ogura T, Yanagihara T, Sakoda S. Expression of the inducible isoform of nitric oxide synthase in the central nervous system of mice correlates with the severity of actively induced experimental allergic encephalomyelitis. J Neuroimmunol. 1995; 62:103–112. [PubMed: 7499486]
66. Zhao W, Tilton RG, Corbett JA, McDaniel ML, Misko TP, Williamson JR, Cross AH, Hickey WF. Experimental allergic encephalomyelitis in the rat is inhibited by aminoguanidine, an inhibitor of nitric oxide synthase. J Neuroimmunol. 1996; 64:123–133. [PubMed: 8632054]
67. Sriram K, O'Callaghan JP. Divergent roles for tumor necrosis factor-alpha in the brain. J Neuroimmune Pharmacol. 2007; 2:140–153. [PubMed: 18040839]
68. Anghelina D, Zhao J, Trandem K, Perlman S. Role of regulatory T cells in coronavirus-induced acute encephalitis. Virology. 2009; 385:358–367. [PubMed: 19141357]
69. Lin MT, Hinton DR, Parra B, Stohlman SA, van der Veen RC. The role of IL-10 in mouse hepatitis virus-induced demyelinating encephalomyelitis. Virology. 1998; 245:270–280. [PubMed: 9636366]
70. Baker BJ, Akhtar LN, Benveniste EN. SOCS1 and SOCS3 in the control of CNS immunity. Trends Immunol. 2009; 30:392–400. [PubMed: 19643666]
71. Kroner A, Schwab N, Ip CW, Ortler S, Gobel K, Nave KA, Maurer M, Martini R, Wiendl H. Accelerated course of experimental autoimmune encephalomyelitis in PD-1-deficient central nervous system myelin mutants. Am J Pathol. 2009; 174:2290–2299. [PubMed: 19443704]
72. Latchman YE, Liang SC, Wu Y, Chernova T, Sobel RA, Klemm M, Kuchroo VK, Freeman GJ, Sharpe AH. PD-L1-deficient mice show that PD-L1 on T cells, antigen-presenting cells, and host tissues negatively regulates T cells. Proc Natl Acad Sci U S A. 2004; 101:10691–10696. [PubMed: 15249675]
73. Ortler S, Leder C, Mittelbronn M, Zozulya AL, Knolle PA, Chen L, Kroner A, Wiendl H. B7-H1 restricts neuroantigen-specific T cell responses and confines inflammatory CNS damage: implications for the lesion pathogenesis of multiple sclerosis. Eur J Immunol. 2008; 38:1734–1744. [PubMed: 18421793]
74. Goverman J. Autoimmune T cell responses in the central nervous system. Nat Rev Immunol. 2009; 9:393–407. [PubMed: 19444307]
75. Kroner A, Schwab N, Ip CW, Leder C, Nave KA, Maurer M, Wiendl H, Martini R. PD-1 regulates neural damage in oligodendroglia-induced inflammation. PLoS One. 2009; 4:e4405. [PubMed: 19197390]
76. Burdeinick-Kerr R, Wind J, Griffin DE. Synergistic roles of antibody and interferon in noncytolytic clearance of Sindbis virus from different regions of the central nervous system. J Virol. 2007; 81:5628–5636. [PubMed: 17376910]
77. Liu T, Khanna KM, Carriere BN, Hendricks RL. Gamma interferon can prevent herpes simplex virus type 1 reactivation from latency in sensory neurons. J Virol. 2001; 75:11178–11184. [PubMed: 11602757]
78. Patterson CE, Lawrence DM, Echols LA, Rall GF. Immune-mediated protection from measles virus-induced central nervous system disease is noncytolytic and gamma interferon dependent. J Virol. 2002; 76:4497–4506. [PubMed: 11932415]
79. Stohlman SA, Bergmann CC, Lin MT, Cua DJ, Hinton DR. CTL effector function within the central nervous system requires CD4+ T cells. J Immunol. 1998; 160:2896–2904. [PubMed: 9510193]
80. Howe CL, Adelson JD, Rodriguez M. Absence of perforin expression confers axonal protection despite demyelination. Neurobiol Dis. 2007; 25:354–359. [PubMed: 17112732]

81. Medana I, Martinic MA, Wekerle H, Neumann H. Transection of major histocompatibility complex class I-induced neurites by cytotoxic T lymphocytes. Am J Pathol. 2001; 159:809–815. [PubMed: 11549572]

82. McPherson SW, Heuss ND, Roehrich H, Gregerson DS. Bystander killing of neurons by cytotoxic T cells specific for a glial antigen. Glia. 2006; 53:457–466. [PubMed: 16355370]

83. Sobottka B, Harrer MD, Ziegler U, Fischer K, Wiendl H, Hunig T, Becher B, Goebels N. Collateral bystander damage by myelin-directed CD8+ T cells causes axonal loss. Am J Pathol. 2009; 175:1160–1166. [PubMed: 19700745]

84. Stohlman SA, Hinton DR, Cua D, Dimacali E, Sensintaffar J, Hofman FM, Tahara SM, Yao Q. Tumor necrosis factor expression during mouse hepatitis virus-induced demyelinating encephalomyelitis. J Virol. 1995; 69:5898–5903. [PubMed: 7637037]

85. Wu GF, Pewe L, Perlman S. Coronavirus-induced demyelination occurs in the absence of inducible nitric oxide synthase. J Virol. 2000; 74:7683–7686. [PubMed: 10906226]

86. Liu Y, Stewart KN, Bishop E, Marek CJ, Kluth DC, Rees AJ, Wilson HM. Unique expression of suppressor of cytokine signaling 3 is essential for classical macrophage activation in rodents in vitro and in vivo. J Immunol. 2008; 180:6270–6278. [PubMed: 18424750]

Abbrevations used in the paper

APC	adenomatous polyposis coli
CLN	cervical lymph nodes
CT	threshold
EAE	experimental allergic encephalomyelitis
HPRT	hypoxanthine-guanine phosphoribosyltransferase
Iba-1	ionized calcium-binding adapter molecule-1
iNOS	inducible nitric oxide synthase
JHMV	neurotropic JHM strain of mouse hepatitis virus
LFB	luxol fast blue
p.i	post-infection
PD-1	programmed death-1
SOCS	suppressor of cytokine signaling

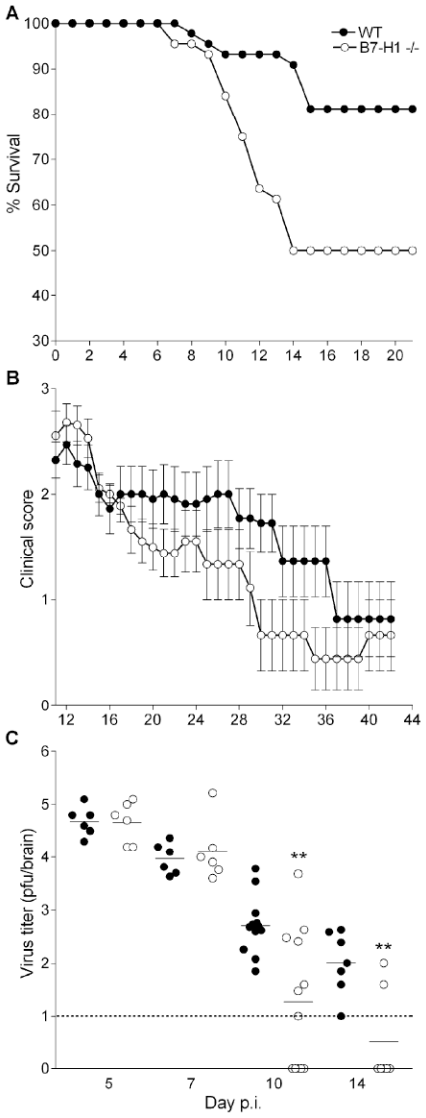

FIGURE 1.

Rapid virus control in B7-H1$^{-/-}$ mice is associated with increased mortality and accelerated recovery in survivors. (*A*) Survival of JHMV infected wt and B7-H1$^{-/-}$ mice (n = 20/group). (*B*) Infected mice (n = 9-11/group) were scored for clinical symptoms at the indicated time points. Data are expressed as the mean ± SEM. (*C*) Virus titers in brains of individual wt and B7-H1$^{-/-}$ mice (n = 6-11/group) were determined by plaque assay. Horizontal bars indicate the mean titer and are representative of three separate experiments. The dashed line marks the limit of detection. Data are on a log^{10} scale. All infected mice had a clinical score ≥ 2. Statistically significant differences between infected wt and B7-H1$^{-/-}$ mice, determined by unpaired *t* test, are denoted by ** ($p < 0.005$).

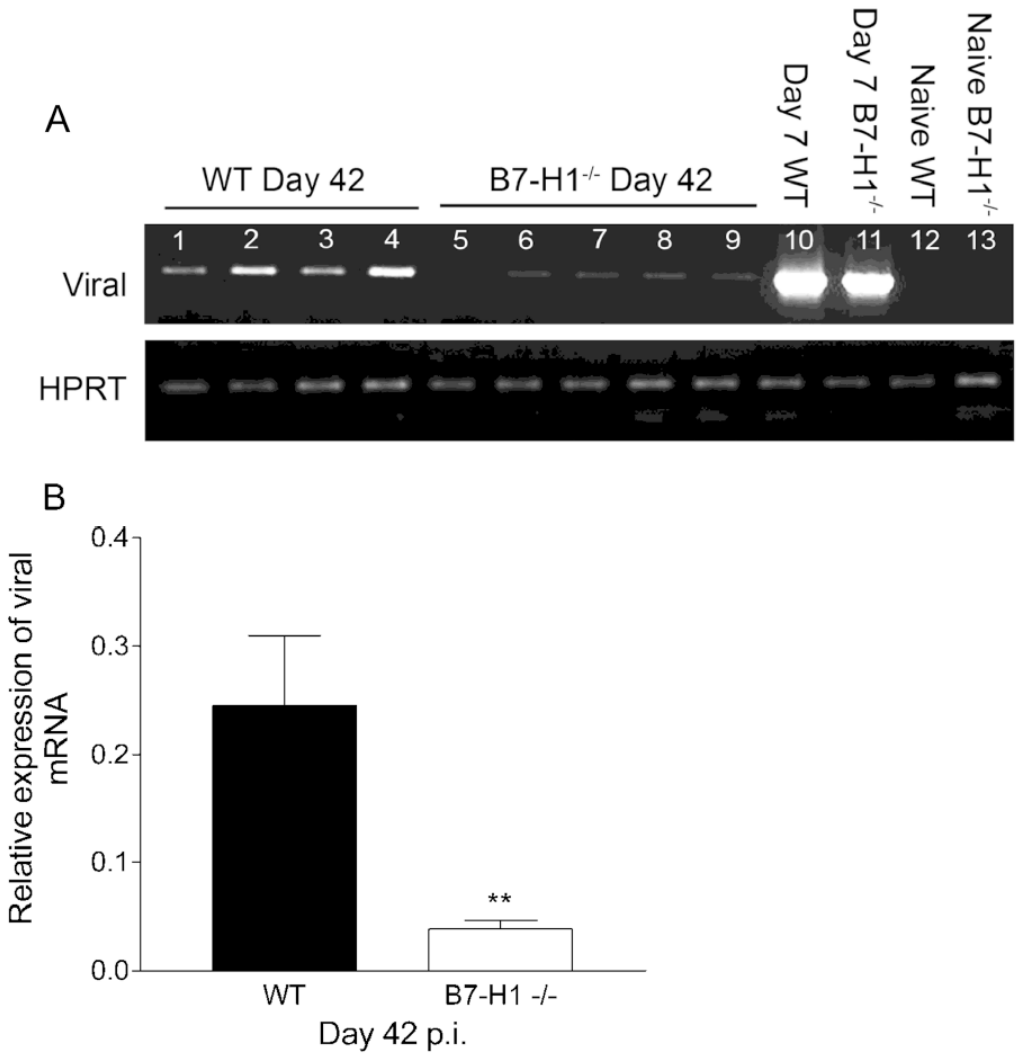

FIGURE 2.

Reduced CNS viral persistence in B7-H1$^{-/-}$ mice. (*A*) Viral mRNA in spinal cords of individual infected wt and B7-H1$^{-/-}$ mice at days 7 and 42 p.i. as well as naive mice amplified by PCR and analyzed by gel electrophoresis. Amplification of HPRT mRNA was used as a control. (*B*) Viral band intensities were measured by densitometry and normalized to HPRT expression. Densitometry data represent mean ± SEM (n = 4-5/group). Statistically significant differences between infected wt and B7-H1$^{-/-}$ mice, determined by unpaired *t* test, are denoted by ** ($p < 0.005$).

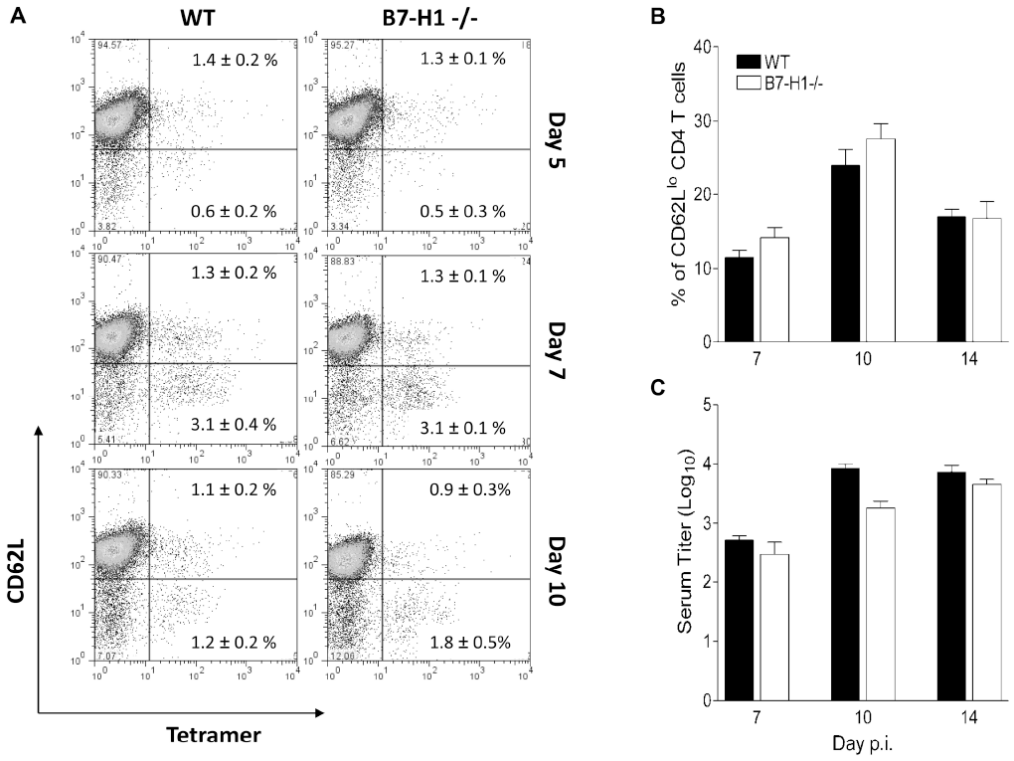

FIGURE 3.

B7-H1 does not alter the frequency of JHMV-specific CD8 T cells, CD62L^{lo} CD4 T cells or serum anti-JHMV Ab in the periphery. (*A* and *B*) CLN cells from infected mice were analyzed for CD4, CD8, CD62L and D^{b}/S510 specific T cell receptor expression by flow cytometry at the indicated days p.i. (*A*) Representative density plots depict staining with D^{b}/S510 tetramer and anti-CD62L Ab. Plots are gated on CD8 T cells. Data are representative of three independent experiments and numbers within each quadrant represent the mean percentages ± SEM of tetramer positive CD8 T cells. Differences between infected wt and B7-H1$^{-/-}$ mice were not statistically significant. (*B*) Data are expressed as the mean ± SEM percentage of CD62L^{lo} CD4 T within the total CD4 T cell population from three independent experiments. (*C*) Kinetics of virus-specific IgG in sera of infected mice assessed by ELISA. Data are expressed as the mean ± SEM (n ≥ 3/group).

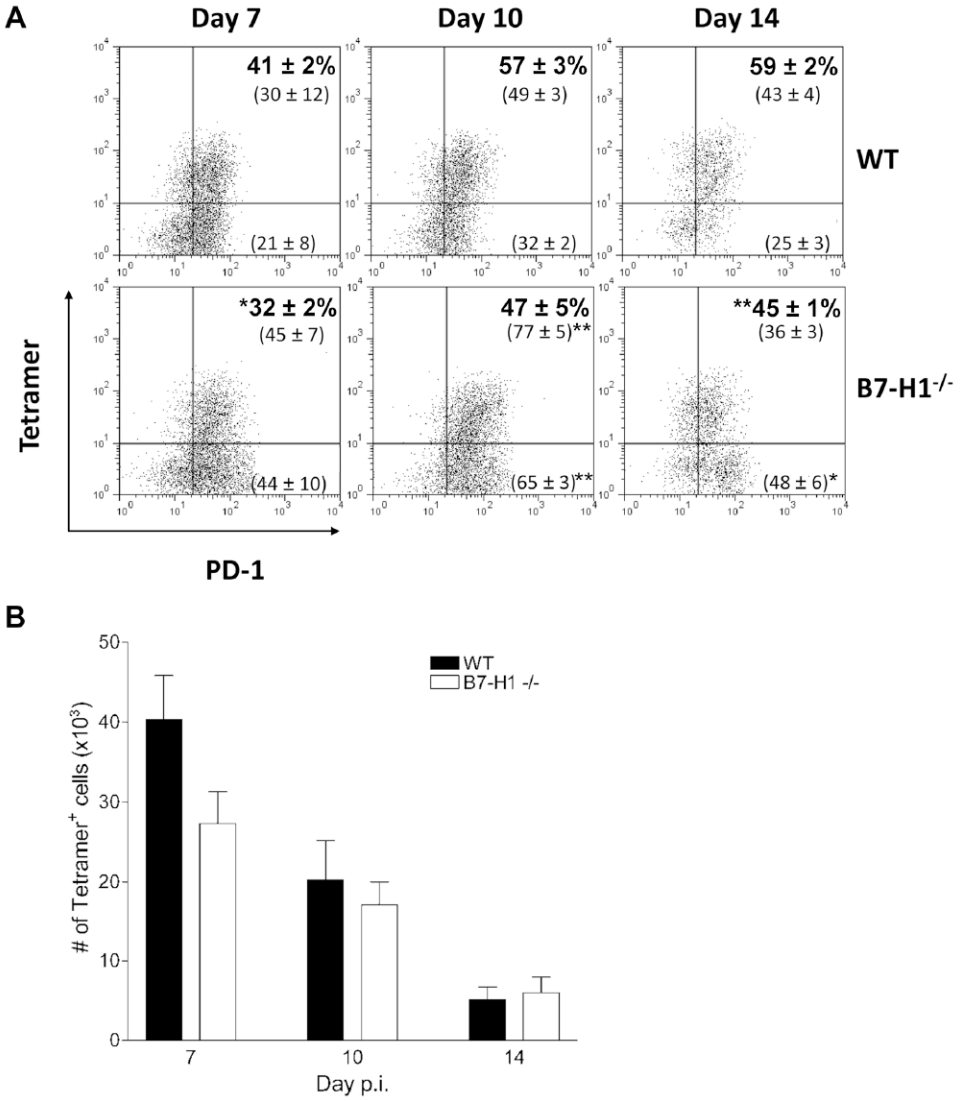

FIGURE 4.

Reduced JHMV-specific CD8 T cells in the CNS of infected B7-H1$^{-/-}$ mice. Cells isolated from the brains of infected mice were analyzed for CD8, PD-1 and D^{b}/S510 specific T cell receptor expression by flow cytometry at the indicated days p.i. (*A*) Representative density plots gated on CD8 T cells depict staining with anti-PD-1 Ab and D^{b}/S510 tetramer. Data are representative of three independent experiments and bold numbers within each quadrant represent the mean percentages ± SEM of tetramer positive CD8 T cells. PD-1 expression on tetramer positive and negative CD8 T cells is indicated by mean fluorescence intensity in parentheses. Data are the mean ± SEM. Statistically significant differences in % of tetramer positive cells and PD-1 expression between infected wt and B7-H1$^{-/-}$ mice, determined by unpaired *t* test, are denoted by * ($p < 0.05$) and ** ($p < 0.005$). (*B*) Total number of tetramer positive CD8 T cells per brain. Data represent the mean ± SEM of two experiments.

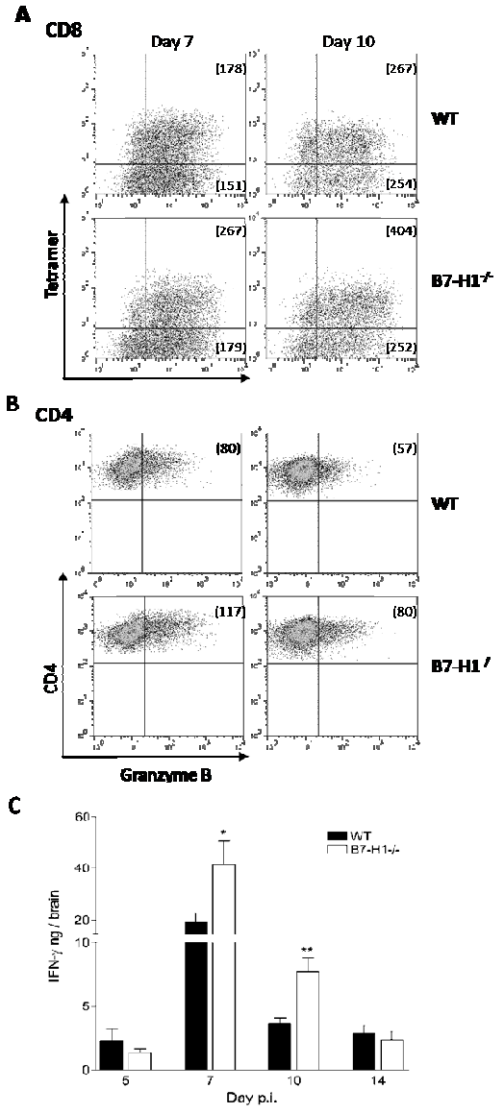

FIGURE 5.

T cell effector functions are enhanced in the absence of B7-H1. (*A* and *B*) Pooled brain cells (n ≥ 4/group) isolated at days 7 and 10 p.i. were stained for CD4, CD8, D^b/S510 specific T cell receptor and intracellular granzyme B. Representative density plots depict staining with (*A*) anti-granzyme B Ab and D^b/S510 tetramer or (*B*) anti-granzyme B and CD4 Ab. Plots are gated on either CD8 or CD4 T cells. Mean fluorescence intensity of granzyme B staining in (*A*) tetramer positive (*upper*) or negative (*bottom*) CD8 T cells or (*B*) CD4 T cells are shown in parentheses. Data are representative of two independent experiments. (*C*) Brain IFN-γ levels were assessed by ELISA at the indicated days p.i. in infected wt and B7-H1$^{-/-}$ mice. Data represent the mean ± SEM (n ≥ 3/group) and are representative of two separate experiments. Statistically significant differences determined by unpaired *t* test, are denoted by * ($p < 0.05$) and ** ($p < 0.005$).

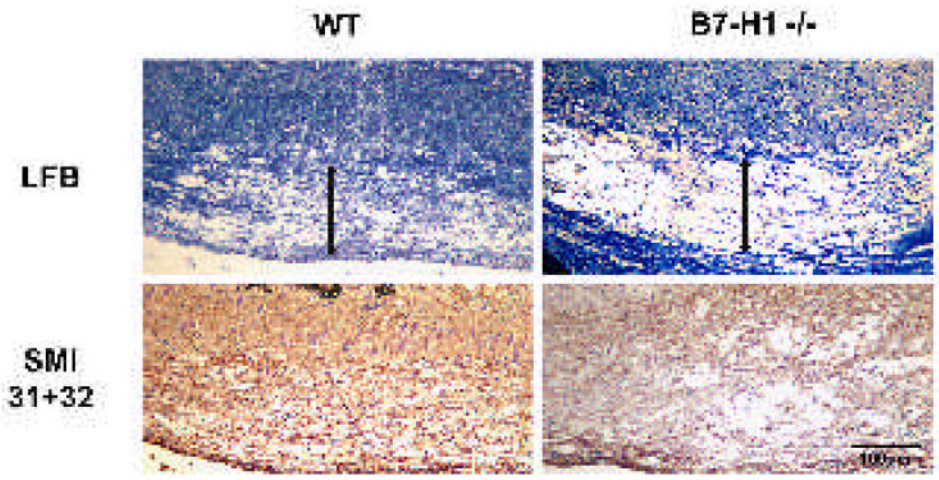

FIGURE 6.

Axonal damage is increased within the demyelinated lesion of B7-H1$^{-/-}$ mice. (*Upper panels*) Spinal cords sections from JHMV infected wt and B7-H1$^{-/-}$ mice at day 10 p.i. stained with LFB to identify areas of myelin loss. Representative lesions are shown with vertical arrows to indicate similar areas of demyelination (*Lower panels*). Axonal integrity within the same spinal cord demyelinated lesions visualized with anti-SMI-31 and -SMI-32 Ab.

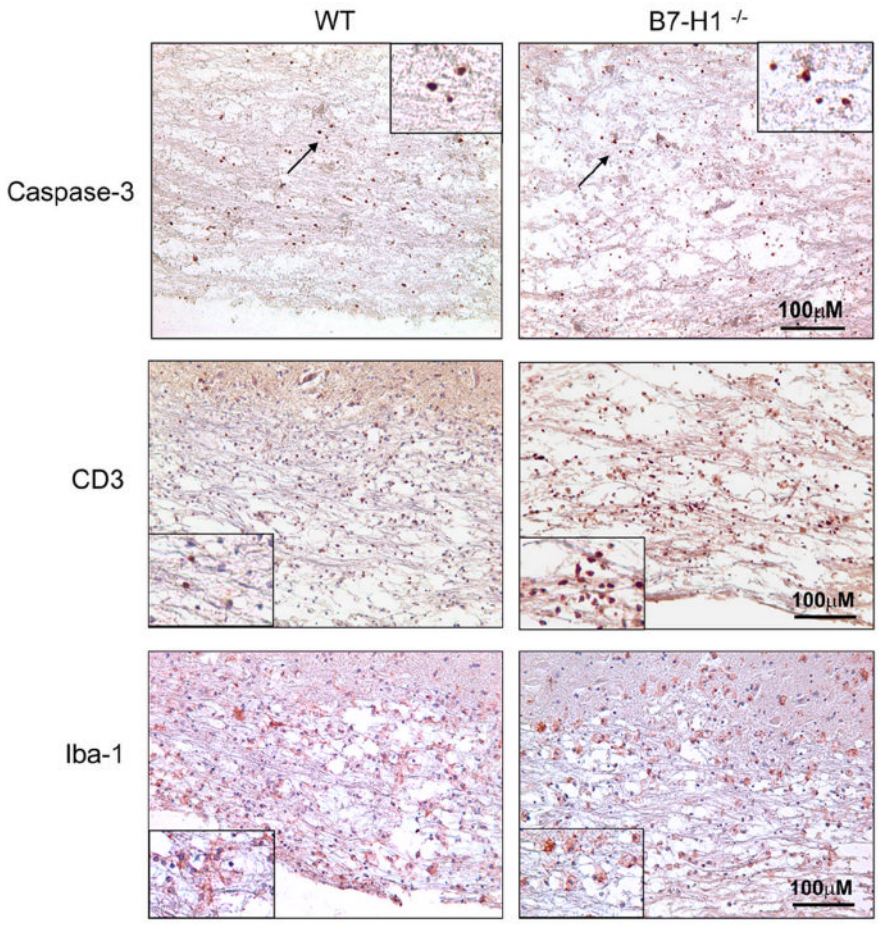

FIGURE 7.

B7-H1 modifies T cell accumulation and microglia/infiltrating monocyte-derived macrophage activation. Sections of spinal cords from JHMV infected wt and B7-H1$^{-/-}$ mice at day 10 p.i. analyzed for apoptosis and inflammation. Apoptotic cells were identified with anti-activated caspase 3 Ab (*Upper panels*), T cells with anti-CD3 Ab (*Middle panels*) and microglia/monocyte-derived macrophages with Iba-1 Ab (*Lower panels*). Inserts show higher magnification of positive cells. Arrows indicate area of insert.

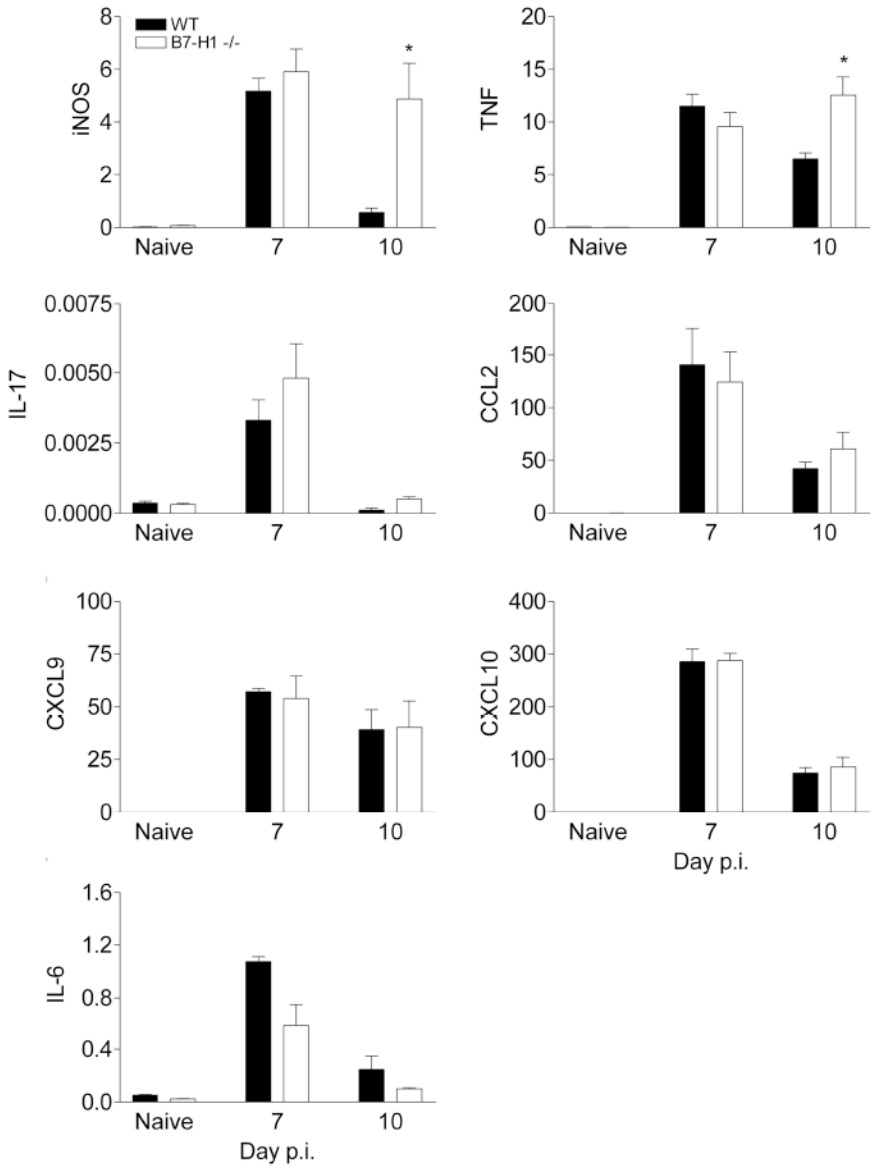

FIGURE 8.

Expression of iNOS and TNF is sustained in the absence of B7-H1. Relative transcript levels of iNOS, TNF, IL-17, CCL2, CXCL9, CXCL10 and IL-6 in spinal cords of naive and infected mice assessed by real-time PCR. Data are expressed as the mean ± SEM transcript level relative to GAPDH mRNA from 3-4 individual mice and are representative of two independent experiments. Statistically significant differences between infected wt and B7-H1$^{-/-}$ mice, determined by unpaired *t* test, are denoted by * ($p < 0.05$).

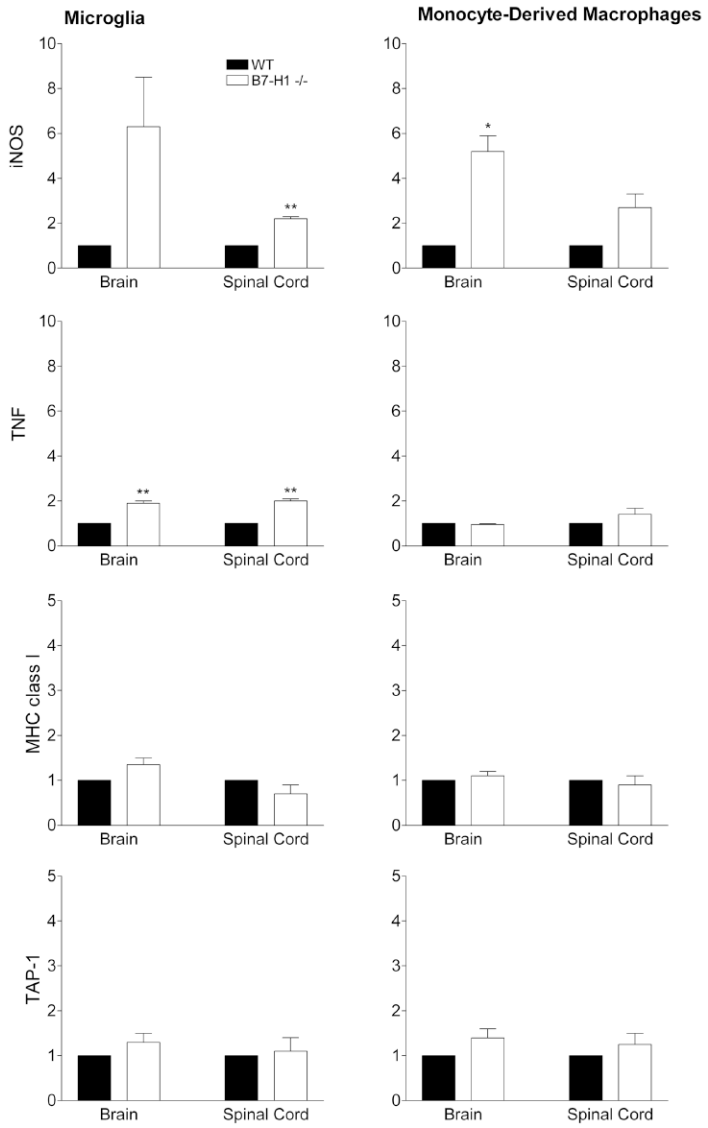

FIGURE 9.

Increased expression of iNOS and TNF by B7-H1$^{-/-}$ microglia/macrophage populations. Relative transcript levels of iNOS, TNF, MHC class I and TAP-1 in purified CD45^{lo} microglia (*Left panels*) and CD45^{hi}CD11b^{+} monocyte-derived macrophages (*Right panels*) from pooled brain or spinal cords 10 days p.i. were assessed by real-time PCR. Transcript levels relative to GAPDH are presented as fold increases with levels from wt mice taken as 1. Data represent the mean ± SEM of two experiments. Statistically significant differences between infected wt and B7-H1$^{-/-}$ mice, determined by unpaired *t* test, are denoted by * ($p < 0.05$) and ** ($p < 0.005$).

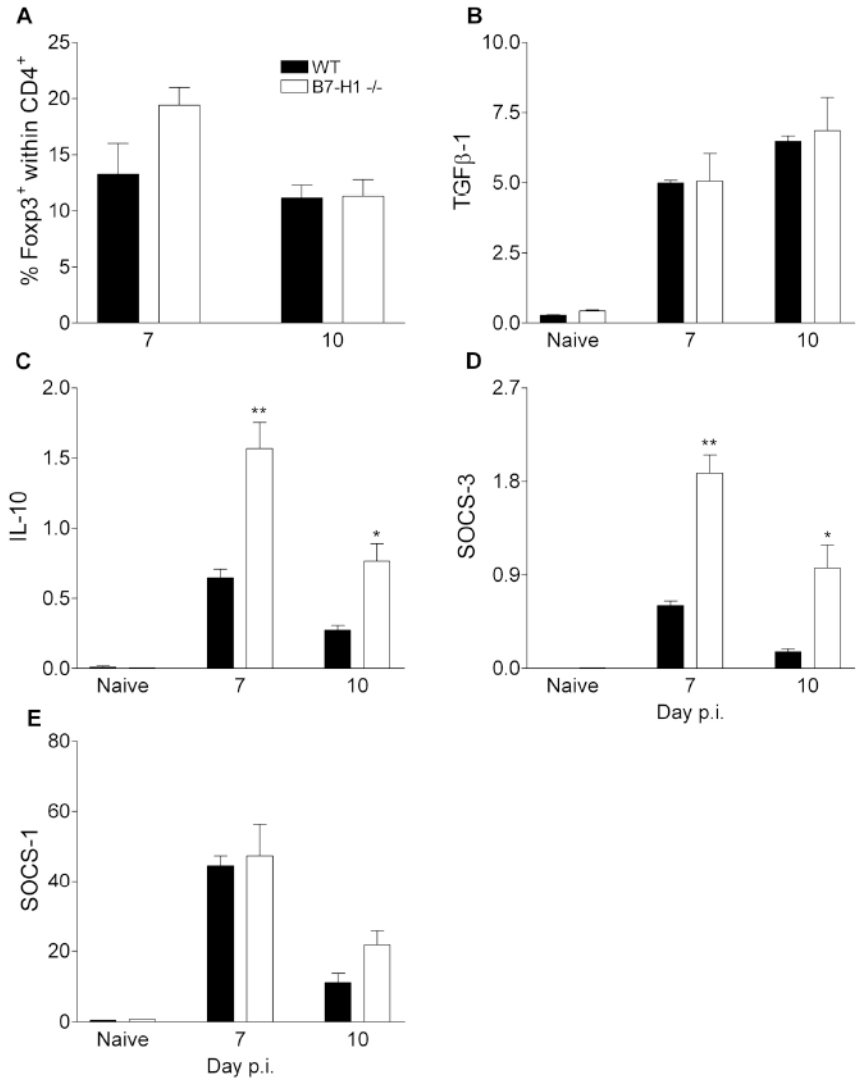

FIGURE 10.

B7-H1 deficiency does not impair anti-inflammatory responses. (*A*) Pooled brain cells (n ≥ 3/group) isolated at days 7 and 10 p.i. were stained for CD4 and intracellular Foxp3. Data represent the mean ± SEM percentage of $Foxp3^+$ cells within the $CD4^+$ T cell population from two independent experiments. (*B-E*) Levels of mRNAs specific for TGFβ-1, IL-10, SOCS-3 and SOCS-1in the spinal cords of naive and infected mice assessed by real-time PCR. Data are expressed as the mean ± SEM transcript level relative to GAPDH mRNA from 3-4 mice. Statistically significant differences between infected wt and B7-$H1^{-/-}$ mice, determined by unpaired *t* test, are denoted by * ($p < 0.05$) and ** ($p < 0.005$). Data are representative of two independent experiments.

Table I

CNS infiltrating cells during JHMV infection of wt and B7-H1$^{-/-}$ mice

Day p.i.	Mice	Cells recovered (× 10^5 / brain)	% CD45^{hi}	% within CD45^{hi} F4/80	CD4	CD8
7	WT	**11.0** ± 1.0	**20.4** ± 1.8	**40.9** ± 3.0	**13.3** ± 0.8	**26.5** ± 0.9
	B7-H1 $^{-/-}$	**10.0** ± 1.0	**20.7** ± 2.5	**41.7** ± 4.4	**15.9** ± 2.2	**28.0** ± 0.7
10	WT	**6.9** ± 1.4	**20.7** ± 4.2	**31.1** ± 2.9	**39.0** ± 7.0	**25.4** ± 3.3
	B7-H1 $^{-/-}$	**8.5** ± 1.7	**19.9** ± 6.2	**30.9** ± 4.4	**28.0** ± 3.3	**31.4** ± 4.3
14	WT	**4.3** ± 0.1	**12.5** ± 3.4	**29.2** ± 2.6	**47.3** ± 7.8	**19.7** ± 1.3
	B7-H1 $^{-/-}$	**5.2** ±1.2	**9.7** ± 3.2	**27.7** ± 0.5	**46.5** ± 9.4	**25.3** ± 4.8

Data presented as mean ± SEM.

Table II

Cytokine expression by CNS infiltrating CD4 and CD8 T cells

Mice[a]	Gene[b,c]	CD8 Tetramer $^{+}$	CD8 Tetramer $^{-}$	CD4
WT	IFN-γ	**104.7** ± 23.6	**20.9** ± 1.5	**229.8** ± 6.4
B7-H1 $^{-/-}$	IFN-γ	**173.1** ± 10.0	**28.5** ± 1.2	**352.9** ± 3.7
WT	TNF	**24.2** ± 2.3	**57.4** ± 0.7	**183.5** ± 3.9
B7-H1 $^{-/-}$	TNF	**39.6** ± 4.3	**60.9** ± 2.4	**111.2** ± 12.3
WT	IL-17	ND[d]	ND[d]	**1.4** ± 0.5
B7-H1 $^{-/-}$	IL-17	ND[d]	ND[d]	**1.1** ± 0.5

[a] Day 7 p.i.

[b] Relative transcript levels normalized to GAPDH mRNA.

[c] Data presented as mean ± SEM.

[d] ND, Not detected.